12

PROJECT SQUID

TECHNICAL REPORT TRW-9-PU

THE COHERENT FLAME MODEL FOR TURBULENT CHEMICAL REACTIONS

BY

FRANK E. MARBLE
CALIFORNIA INSTITUTE OF TECHNOLOGY
CONSULTANT, TRW DEFENSE AND SPACE SYSTEMS GROUP

and

JAMES E. BROADWELL
TRW DEFENSE AND SPACE SYSTEMS GROUP

PROJECT SQUID HEADQUARTERS
CHAFFEE HALL
PURDUE UNIVERSITY
WEST LAFAYETTE, INDIANA 47907

JANUARY 1977

Project SQUID is a cooperative program of basic research relating to Jet Propulsion. It is sponsored by the Office of Naval Research and is administered by Purdue University through Contract N00014-75-C1143, NR-098-038.

Technical Report TRW-9-PU

PROJECT SQUID

A COOPERATIVE PROGRAM OF FUNDAMENTAL RESEARCH
AS RELATED TO JET PROPULSION
OFFICE OF NAVAL RESEARCH, DEPARTMENT OF THE NAVY

THE COHERENT FLAME MODEL FOR TURBULENT CHEMICAL REACTIONS

by

Frank E. Marble
California Institute of Technology
Consultant, TRW Defense and Space Systems Group

and

James E. Broadwell
TRW Defense and Space Systems Group

January 1977

PROJECT SQUID HEADQUARTERS
CHAFFEE HALL
PURDUE UNIVERSITY
WEST LAFAYETTE, INDIANA

See 1473

THE COHERENT FLAME MODEL FOR TURBULENT CHEMICAL REACTIONS

Abstract

A description of the turbulent diffusion flame is proposed in which the flame structure is composed of a distribution of laminar diffusion flame elements, whose thickness is small in comparison with the large eddies. These elements retain their identity during the flame development; they are strained in their own plane by the gas motion, a process that not only extends their surface area, but also establishes the rate at which a flame element consumes the reactants. Where this flame stretching process has produced a high flame surface density, the flame area per unit volume, adjacent flame elements may consume the intervening reactant, thereby annihilating both flame segments. This is the flame shortening mechanism which, in balance with the flame stretching process, establishes the local level of the flame density. The consumption rate of reactant is then given simply by the product of the local flame density and the reactant consumption rate per unit area of flame surface. The proposed description permits a rather complete separation of the turbulent flow structure, on one hand, and the flame structure, on the other, and in this manner permits the treatment of reactions with complex chemistry with a minimum of added labor. The structure of the strained laminar diffusion flame may be determined by analysis, numerical computation, and by experiment without significant change to the model.

The flame density and the mass fractions of reactant are described by non-linear diffusion equations in which those equations for the reactants each contain a consumption or production term proportional to the local flame density. The flame density equation contains a production term associated with flame surface stretching and a consumption term describing the flame shortening by mutual annihilation. Each of the equations contains a turbulent diffusion term utilizing a scalar diffusivity. The model of inhomogeneous turbulence, proposed by Saffman, completes the description of the problem and couples with the flame and composition equations to determine the velocity distribution and the turbulent diffusivity. A single additional universal constant, over those appearing in Saffman's model, is required in the model equations for the flame.

The coherent flame model has been applied to diffusion flame structure in the mixing region between two streams and predicts correctly the result that the reactant consumption per unit length of flame is independent of the distance from the initiation of mixing. In this example which is carried out for small density changes, both the fluid mechanical and flame variables possess similarity solutions.

The coherent flame model is also applied to the turbulent fuel jet which clearly does not have a similarity solution simply because the finite mass flow of fuel is eventually consumed. The problem is solved utilizing an integral technique and numerical integration of the resulting differential equations. The model predicts the flame length and superficial comparison with experiments suggest a value for the single universal constant. The theory correctly predicts the change of flame length with changes in stoichiometric ratio for the chemical reaction.

TABLE OF CONTENTS

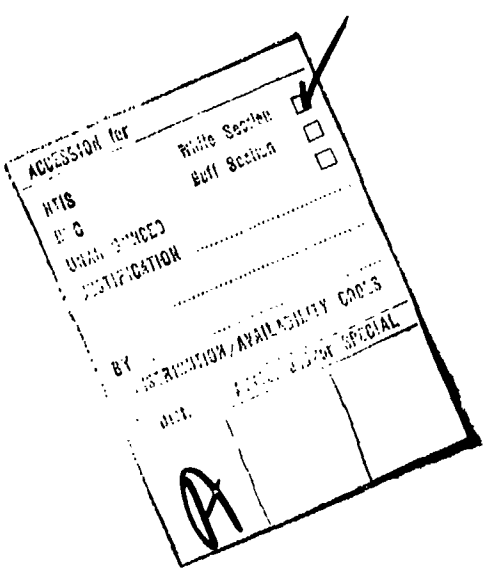

1. INTRODUCTION

Some of the earliest considerations of turbulent combustion processes, e.g., Damköhler,[1] Shchelkin,[2] included the suggestion that a turbulent combustion field consists of a collection of laminar flame surfaces in which the laminar flame structure retains its identity while being distorted by the turbulent motion. This conjecture found additional support a decade later in the work of Hawthorne, et al.,[3] Hottel,[4] Karlovitz, et al.[5] Wohl,[6] and others. That brief period provided some provacative experiments through schlieren photographs[7] and ion probe measurements[8] that demonstrated the presence of concentrated reaction zones in turbulent flames. Looking back on some of these experiments, e.g., Hottel,[9] Zukoski,[10] we find clear evidence of the large structure of inhomogeneous turbulence that, until the recent work of Brown and Roshko,[11] escaped the attention of workers in turbulence research. This early interest in a possible laminar flame structure within turbulent combustion zones stimulated no serious steps toward a qualitative formulation of these ideas; rather, subsequent theoretical developments were guided by the Reynolds,[12] Taylor,[13] Kármán,[14] tradition and, as a consequence, treated the local reaction rates in terms of mean values of products of fluctuating state quantities. Each viewpoint has its merits; each has its advantage in interpreting the effects of certain portions of the turbulence spectrum, a fact that was clearly noted by Damköhler[1] and Shchelkin.[2]

It is the aim of the present work, which extends an analysis carried out by the present authors[15] with support of the Air Force Weapons Laboratory, to develop an analytical formulation to the concept of a turbulent flame consisting of coherent laminar flame elements, where by coherent, it is implied that a local laminar flame element retains its identity although it is severely distorted and strained by the turbulent motions. More specifically, the thickness of the diffusion flame is assumed small in comparison with the wave length of prominent disturbances in the gas. Then the local flame element is stretched and distorted by the local gas rotation and strain rate, but the diffusion flame structure is affected only by the strain rate in its own plane.

According to this physical picture, the rate at which reactants are consumed, in volume of dimensions small compared with the physical problem but large with respect to laminar flame thickness, is the product of flame surface area and reacting consumption rate per unit flame surface. A simplified illustration of this process is shown in Figure 1 for a mixing zone. The straining associated with the diffusive character of turbulence not only leads to the growth of flame surface area but is essential in determining the reactant consumption per unit of flame surface. A greater reaction rate is associated with a "stretching" diffusion flame because the straining in the plane of the flame induces a flow of gas toward the reaction line steepening the concentration gradients and thus augmenting the diffusion of reactants to the flame.

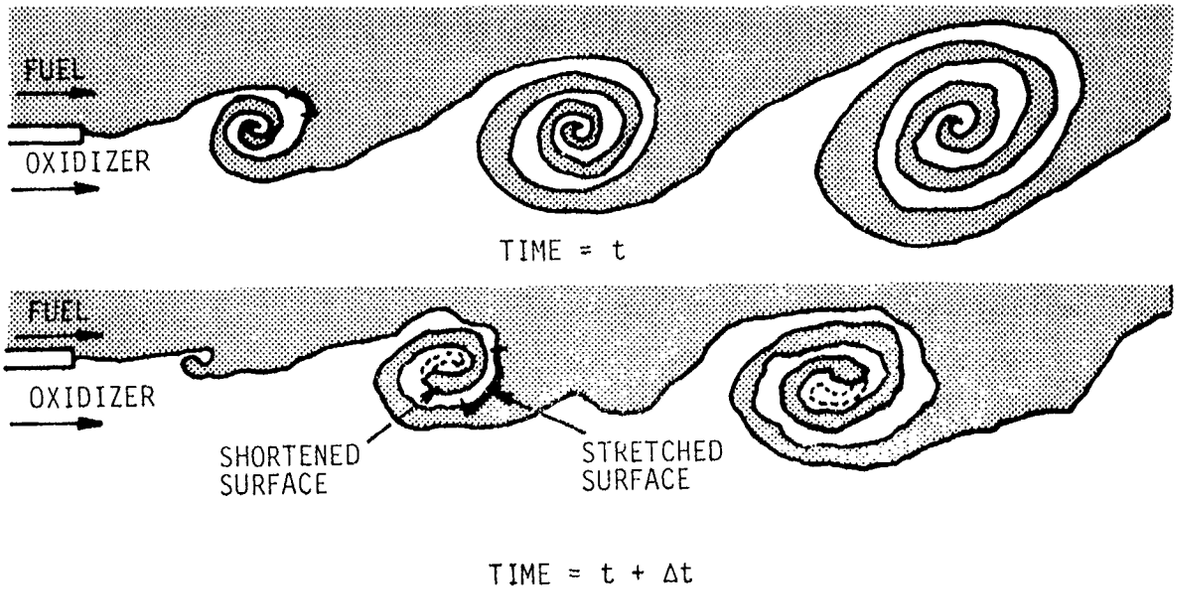

Figure 1. Schematic Drawing of Flame Surface Stretching and Shortening.

As the straining motion continues to increase the flame surface, regions develop where flame fronts move so close to one another that they interact, Figure 1. In time, the two neighboring flame elements move together, consume the intervening reactant and destroy these two elements of flame surface. This is the flame shortening mechanism that eventually balances the extension caused by straining, and it is an essential feature that was notably absent from earlier intuitive discussions of the flame element model of turbulent

combustion. It is necessary that in the combustion of unmixed reactants, the competition between i) flame surface growth by straining and ii) flame surface reduction by mutual annihilation of reaction fronts, establishes the level of reactant consumption per unit volume.

A particularly attractive feature of the coherent flame model is the effective separation of the details of the chemistry from the details of the turbulent structure. The chemistry appears only in the plane laminar diffusion flame subjected to strain rate, a calculation in which complex chemistry may be incorporated with relative ease. The turbulent structure, on the other hand, only involves the heat release in its response to the corresponding density changes. Thus, the description of the turbulence and the description of chemistry and thermodynamics of the reaction are coupled in a rather elementary way; when the heat of reaction is low, the coupling is correspondingly weak.

A formulation of the coherent flame model for the turbulent diffusion flame then requires i) a model for inhomogeneous turbulence, including closure conditions; ii) a model for flame surface distribution over the turbulent region, which leads to a corresponding reactant consumption and heat release; and iii) calculation or measurement of the reactant consumption rate for a laminar diffusion flame that is undergoing strain in its own plane.

In the following sections, an analytical formulation for this model is suggested and some general properties are discussed. The equations are then applied, for very rapid reaction rates and low heat releases, to the problems of the turbulent mixing layer and the turbulent fuel jet.

2. THE COHERENT FLAME MODEL

According to the coherent flame model for turbulent diffusion flames, the flowfield is divided into two regions by a flame sheet, one of the reactants existing on each side of the sheet. The sheet becomes extensively distorted and dispersed during the turbulent combustion process and it is, therefore, appropriate to define a field variable $\Sigma(x_i,t)$ which specifies the flame surface area per unit volume. This quantity is denoted the flame density and has the dimension of a reciprocal length. All of the chemical reaction takes place within a region that is small in comparison with the predominant length which describes the distortion of the flame front. We know that in a laminar diffusion flame, such as that represented by the flame sheet, the combustion products remain within the diffusion layer, a layer which under the most elementary circumstances grows as $\sqrt{t}$. The situation is different when the turbulent motion is continually extending the flame surface, say at a linear strain rate ε, and in such a flame, the diffusion zones quickly stabilize at a thickness proportional to $\varepsilon^{-1/2}$. The newly-formed reaction products then remain within this small distance of the flame sheet and are distributed over the geometric mixing zone by the extension and migration of the flame sheet. In the volume for which the flame density is $\Sigma(x_i,t)$, we may similarly define mass fractions $\kappa_1(x_i,t)$, $\kappa_2(x_i,t)$ of the reactants, the mass fraction $\kappa_3(x_i,t)$ of the reaction products, and a mass fraction $\kappa_4(x_i,t)$ of an inert diluent.

If the process of flame extension were to continue without modification, the flame surface would become dense in some regions and the spacing between surfaces, which on the average is Σ^{-1}, would be of the same order as the thickness of the flame diffusion zones. In this event, neighboring flame sheets are no longer isolated; they interact and quickly consume the intervening reactant.[16] This process shortens the flame surface and, hence, reduces the flame surface density at a rate proportional to the volume rate of reactant consumption by a unit area of the flame, V_D, and inversely proportional to the distance between the two flame fronts bounding the reactant in question. Now the distance between flame fronts that is occupied by a particular species is of the order of the volume fraction of that species divided by the flame surface per unit volume. Then for the species with

volume fraction v_i, the effective distance between flame fronts occupied by the i^{th} chemical species is v_i/Σ. But is proves convenient to describe this in terms of mass fractions κ_i and the molecular weights M_i of the species, $v_i = (\kappa_i/M_i)(\sum \kappa_j/M_j)^{-1}$, so that the characteristic length associated with the i^{th} chemical species is

$$\frac{\kappa_i}{M_i}/\Sigma \sum \kappa_j/M_j$$

It should be noted here that when the molecular weights of the reactants and products are nearly equal, that is $M_1 = M_2 = M_3$, then $(\sum \kappa_j/M_j)\, M_i = 1$ and the above characteristic length becomes $= \kappa_i/\Sigma$, a form that we shall employ in later calculations.

With this result, we may establish the physical order of the rate of flame surface reduction due to the consumption of the i^{th} reactant as

$$\frac{V_{Di}}{v_i}\,\Sigma$$

per unit of flame surface, or

$$\frac{V_{Di}}{v_i}\,\Sigma^2 \qquad (1)$$

per unit of volume that contains a flame area Σ. We shall write the flame surface reduction caused by consumption of the fuel and oxidizer components, $i = 1$ and $i = 2$, as the sum of terms of the type given by expression 1.

Now it is a matter of formal calculation to obtain an equation for the change in area of an element associated with fluid particles, as it is stretched and deformed by a turbulent medium. In fact, Batchelor[17] has done exactly this calculation in examining the behavior of line segments and surface elements in homogeneous isotropic turbulence. For our purposes, the result states that the Eulerian time derivative of Σ is given by the sum of the turbulent diffusion of this quantity and the increase of flame density

by the local strain rate of the mean motion. It is presumed that, for inhomogeneous turbulence, the strain rate of the mean motion is sufficiently dominant that the additional straining associated with turbulent fluctuations may be neglected. For two reasons, this result does not describe accurately the behavior of a flame element. First, the flame front generally moves with respect to the fluid and thus does not always contain the same fluid particles. Second, the flame shortening mechanism, in which adjacent flame fronts consume the intervening reactant and annihilate each other, must be accounted for. They are two aspects of the same differences which contrast the behavior of the flame sheet with that of a surface element consisting of the same fluid elements. The first of these will be neglected in our formulation while the second, and dominant, effect will be accounted for by shortening mechanisms discussed above.

Then in a turbulent fluid field with mean velocity components U_i, scalar turbulent diffusivity $\mathcal{D}$ and local scalar mean strain rate ϵ, we postulate that the flame surface density satisfies the partial differential equation

$$\frac{\partial \Sigma}{\partial t} + U_k \frac{\partial \Sigma}{\partial x_k} = \sigma \frac{\partial}{\partial x_k}\left(\mathcal{D} \frac{\partial \Sigma}{\partial x_k}\right) + \epsilon \Sigma - \left(\sum \frac{V_{Dj}}{V_j}\right) \Sigma^2 \qquad (2)$$

where the specific subscripts $j = 1$ and $j = 2$ will denote the "fuel" and "oxidizer" reactants, respectively.

A notable advantage of the coherent flame model, upon which we shall elaborate later, is that the chemical reaction rate may be expressed in terms of the local flame surface density. Thus, for example, the mass of species 1 that is being consumed per unit volume is just $\rho V_{D1} \Sigma$ since V_{D1} is volume consumption rate of fuel by a unit flame area. Then by well known techniques, we write the continuity equation for the fuel constituent in a turbulent flow

$$\frac{\partial \kappa_2}{\partial t} + U_k \frac{\partial \kappa_2}{\partial x_k} = \sigma^* \frac{\partial}{\partial x_k}\left(\mathcal{D} \frac{\partial \kappa_1}{\partial x_k}\right) - V_{D1} \Sigma \qquad (3)$$

and similarly for the oxidizer component,

$$\frac{\partial \kappa_2}{\partial t} + U_k \frac{\partial \kappa_2}{\partial x_k} = \sigma_* \frac{\partial}{\partial x_k}\left(\mathcal{D} \frac{\partial \kappa_2}{\partial x_k}\right) - V_{D2}\, \Sigma \tag{4}$$

where σ^* is an appropriate turbulent Schmidt number. Because $\sum \kappa_j = 1$, the remaining species conservation equation is unnecessary so long as the inert diluent may be grouped with other species or is absent. It is assumed, of course, that the reactant consumption rates V_{D1}, V_{D2} for a unit flame area are available in terms of the local variables and transport properties. The reactant consumption rate may, in the case of the complex chemistry, require a numerical calculation or, in the case of rapid kinetics which we shall examine subsequently in more detail, it may be expressed analytically in a simple closed form. Under any circumstances, the quantity of importance, V_{D1}, is obtained from a one-dimensional calculation that is independent of the detailed solution of the partial differential equations describing the turbulent flame.

To complete the formulation, a model for inhomogeneous turbulence is required which yields, in addition to the velocity field, the scalar diffusivity and the scalar straining rate ϵ. The model that is the most closely related is that suggested by Saffman[18] which utilizes the specific vorticity $|\omega|$ and the specific turbulent kinetic energy as independent variables, employs a scalar diffusivity and recognizes the role of the local magnitude of the straining motion in the mechanism for producing both vorticity and energy. Then for an incompressible medium, implying that the heat of reaction is small, this model gives

$$\frac{\partial U_k}{\partial x_k} = 0 \tag{5}$$

$$\frac{\partial U_i}{\partial t} + U_k \frac{\partial U_i}{\partial x_k} = -\frac{1}{\rho}\frac{\partial p}{\partial x_i} + \frac{\partial}{\partial x_k}\left\{\mathcal{D}\left(2S_{ik}\right)\right\} \tag{6}$$

$$\frac{\partial e}{\partial t} + U_k \frac{\partial e}{\partial x_k} = \sigma^* \frac{\partial}{\partial x_k}\left(\mathcal{D} \frac{\partial e}{\partial x_k}\right) + \alpha^* \sqrt{(2\, S_{ij})^2}\, e - \beta^* \omega\beta \qquad (7)$$

$$\frac{\partial \omega^2}{\partial t} + U_k \frac{\partial \omega^2}{\partial x_k} = \sigma \frac{\partial}{\partial x_k}\left(\mathcal{D} \frac{\partial \omega^2}{\partial x_k}\right) + \alpha \sqrt{\left(\frac{\partial U_i}{\partial x_j}\right)^2}\, \omega^2 - \beta\omega \cdot \omega^2 \qquad (8)$$

The first two equations are of the standard form, and it is assumed that the Reynolds stresses -- as well as other diffusion processes -- may be described by a scalar turbulent diffusivity $\mathcal{D}$. It is a familiar dimensional argument that the turbulent diffusivity, which has the dimension of a velocity times a length, may be constructed from local field quantities; in fact, this is the essence of Kármán's original concept of mechanical similitude.[19] In the model we use, Saffman chooses the turbulent energy density e (ℓ^2/t^2) and the magnitude ω of the vorticity (1/t) as the local physical quantities. Both turbulent kinetic energy and vorticity have physically understood transport laws, and they are related through the association of the turbulent velocities with the vorticity that induces them. Then take

$$\mathcal{D} \equiv e/\omega \qquad (9)$$

which not only defines the turbulent diffusivity, but establishes a magnitude relationship between e and ω.

The transport Equation 7 for the turbulent energy has a physically recognizable form; the three terms on the right-hand side are, in order: diffusion, production, and dissipation. The turbulent diffusion term is clear and the production term is patterned after the one which occurs naturally in turbulence theory which is proportional to the Reynolds stresses acting on the mean strain rates. Here, e is taken as a measure of the Reynolds stress, which $\frac{1}{2}$ ($\partial U_i/\partial x_j + \partial U_j/\partial x_i$) is the strain rate of the mean flow, and we have denoted it S_{ij}. The last term, the dissipation, must be constructed from the product of three fluctuating velocities, and Saffman has chosen this to be the product of vorticity and turbulent energy. The vorticity equation 8 is reminescent of Helmholtz vortex equations and may be intuitatively argued from them. Again, the turbulent diffusion of

vorticity is described by the diffusivity $\mathcal{D}$. The second term represents the production of vorticity by vortex stretching, the stretching being given in Saffman's model by the magnitude of the velocity gradient tensor. It should be noted that the mean velocity derivatives enter differently in the energy and vorticity production terms, Saffman,[18] and it is only for certain flowfields that the two become indistinguishable.

This set of four equations, 5 through 8, results from a complete model in the sense that the constants involved are universal, closure being achieved by the choice of turbulent diffusivity $\mathcal{D} \equiv e/\omega$. In the original formulation of the coherent flame model presented in Reference 15, closure was achieved by identifying the turbulent diffusivity $\mathcal{D}$ as the product of a characteristic velocity and a characteristic length defined locally or globally. The fact that this choice must be made with some physical insight, and differently for each type of flow, shows that the problem is not described completely by the differential equations; such a model is sometimes denoted incomplete, implying that, when coupled with the coherent flame model, the coefficients σ, σ^*, etc. are not universal but may require adjustment from one flow type to another.

3. REACTANT CONSUMPTION RATE

The reactant consumption rates enter into the problem in the form V_{D1} and V_{D2}, the volume of fuel and oxidizer consumed per unit flame area, respectively, and play roles both in the species conservation relations and in the equations describing the flame surface density. These quantities are assumed to be determined locally by the flame structure and to depend only upon local quantities; in particular, for the diffusion flame, they are determined by fuel and oxidizer concentrations and a local fluid mechanical property. As shall be illustrated, they may be determined analytically, or by numerical calculations when the kinetics are complicated and have an essential effect. The important point to keep in mind is that the entire flame structure and chemical kinetics are coupled with the field analysis rather weakly, so that the consideration of complex kinetics complicates only the local flame structure and not the formulation of the flowfield and the flame distribution.

As a first illustration, consider the diffusion flame with rapid kinetics; in this approximation the reaction takes place at a surface of infinitesimal thickness. Utilizing the coordinates x and y to signify distances parallel to and normal to the flame surface, supposed to lie along $y = 0$, the fuel and oxidizer concentrations satisfy the equations

$$\frac{\partial \kappa_1}{\partial t} + u \frac{\partial \kappa_1}{\partial x} + v \frac{\partial \kappa_1}{\partial y} = \frac{1}{\rho} \frac{\partial}{\partial y} \left(\rho D \frac{\partial \kappa_1}{\partial y} \right) \tag{10}$$

$$\frac{\partial \kappa_2}{\partial t} + u \frac{\partial \kappa_2}{\partial x} + v \frac{\partial \kappa_2}{\partial y} = \frac{1}{\rho} \frac{\partial}{\partial y} \left(\rho D \frac{\partial \kappa_2}{\partial y} \right) \tag{11}$$

where

$$\frac{\partial u}{\partial x} + \frac{\partial v}{\partial y} = 0 \tag{12}$$

when the heat of reaction is negligible and the gas density ρ is a constant. For the classical diffusion flame, the field is independent of x, but the solution is time dependent. Then, since $\frac{\partial u}{\partial x} = 0$, $v = v(t)$ which, as will appear, is not generally zero. Then introducing the variable

$$\xi = \frac{y}{\sqrt{Dt}} \tag{13}$$

and taking

$$v(t) = W\sqrt{\frac{D}{t}} \tag{14}$$

the species conservation equations are reduced to a similarity form and become

$$\frac{d^2\kappa_i}{d\xi^2} + \left(\frac{\xi}{2} - W\right)\frac{d\kappa_i}{d\xi} = 0 \tag{15}$$

where i = 1, 2 for fuel or oxidizer, respectively. This pair of differential equations is required to satisfy the conditions that the fuel and oxidizer mass fractions take on the values $\kappa_1(\infty)$ and $\kappa_2(-\infty)$ at $y = +\infty$ and $y = -\infty$, respectively and that the mass flux to the diffusion flame, $y = 0$, supplies fuel and oxidizer in the stoichiometric ratio. This latter condition is explicitly

$$\frac{\rho D \frac{\partial \kappa_1}{\partial y}(0,t)}{-\rho D \frac{\partial \kappa_2}{\partial y}(0,t)} = f \tag{16}$$

where f is the known, constant stoichiometric fuel-oxidizer ratio. It is not difficult to show that

$$\kappa_1 = \kappa_1(\infty)\,\frac{\text{erf}\left(\frac{\xi}{2} - W\right) + \text{erf}\,(W)}{1 + \text{erf}\,(W)} \tag{17}$$

and

$$\kappa_2 = \kappa_2(-\infty)\,\frac{\text{erf}\left(-\frac{\xi}{2} + W\right) - \text{erf}\,(W)}{1 - \text{erf}\,(W)} \tag{18}$$

satisfying the differential Equation 15 and the boundary conditions at $y = \pm\infty$. The stoichiometry condition (Equation 16) then determines the

characteristic value W, and it is a matter of calculation to show that this gives the result

$$\frac{\kappa_1(\infty)\ \left(1 - \text{erf}\ (W)\right)}{\kappa_2(-\infty)\ \left(1 + \text{erf}\ (W)\right)} = f \tag{19}$$

Now $\kappa_1(\infty)/\kappa_2(-\infty)$ is the imposed fuel-oxidizer ratio of the problem, and the quotient of this with the stoichiometric fuel-oxidizer ratio

$$\frac{\kappa_1(\infty)/\kappa_2(-\infty)}{f} \equiv \phi \tag{20}$$

is frequently called the equivalence ratio. Thus, the value of W becomes

$$W = \text{erf}^{-1}\left(\frac{\phi - 1}{\phi + 1}\right) \tag{21}$$

This quantity defines the value of the transverse gas velocity

$$v(t) = \sqrt{\frac{D}{t}}\ \text{erf}^{-1}\left(\frac{\phi - 1}{\phi + 1}\right) \tag{22}$$

which is required to keep the flame stationary at the x-axis. With this solution, the values of the reactant volume consumption rates may be calculated as

$$V_{D1} = \kappa_1(\infty)\ \sqrt{\frac{D}{\pi t}}\left(\frac{\phi + 1}{2\phi}\right)e^{-W^2} \tag{23}$$

and

$$V_{D2} = \kappa_2(-\infty)\ \sqrt{\frac{D}{\pi t}}\left(\frac{\phi + 1}{2}\right)e^{-W^2} \tag{24}$$

This result exhibits the intuitively clear result that the consumption rates decrease with increasing time, because the diffusion layers that supply the reactants grow thicker with time. The equivalence ratio, which

determines the value of W, is known because $\kappa_1(\infty)$ and $\kappa_2(-\infty)$ are equal to the values remote from the turbulent flame since the diffusion zone thickness is assumed small in comparison with flame front spacing. At any point within the turbulent flame, therefore, the reactant consumption rates are known in terms of the time t elapsed since the formation of the flame.

In disucssing the turbulent flame structure earlier, it was emphasized that the turbulent motions tend to extend the flame surface and that the significant part of this extension consists of strain rate in the plane of the flame. Now, if the flame is aligned with the x-axis and the remaining axes chosen so that straining rate is along the x-axis, the resulting strained diffusion flame is also directly soluble. In the particular instance when the straining rate in the fluid is large, i.e., where

$$\varepsilon \equiv \frac{\partial u}{\partial x} \tag{25}$$

is large and constant, Equations 10 through 14 take the form

$$\frac{\partial \kappa_i}{\partial t} + v \frac{\partial \kappa_i}{\partial y} = \frac{\partial}{\partial y}\left(D \frac{\partial \kappa_i}{\partial y}\right) \tag{26}$$

and

$$\varepsilon + \frac{\partial v}{\partial y} = 0 \tag{27}$$

If we solve the problem as previously posed, the solution has a brief transient followed by a steady solution which we may obtain be neglecting $\partial \kappa_i / \partial t$ and taking v and κ_i to be functions of y only. Then introducing the variable

$$\xi \equiv \frac{y}{\sqrt{D/2\varepsilon}} \tag{28}$$

$$v = -\varepsilon y + \sqrt{2\varepsilon D}\, W \tag{29}$$

with W unknown, the differential equation 26 becomes

$$\frac{d^2\kappa_i}{d\xi^2} + \left(\frac{\xi}{2} - W\right)\frac{d\kappa_i}{d\xi} = 0 \tag{30}$$

formally identical with Equation 15. The conditions for $y \pm \infty$, as well as stoichiometry condition at the flame front, are also identical with those of the time-dependent flame, and, hence, the solution for the strained flame is likewise given by Equations 17 and 18 together with W evaluated by Equation 21, but with ξ as defined in Equation 28. The corresponding volume consumption rates of reactants are easily calculated

$$V_{D1} = \kappa_1(\infty)\ \sqrt{\frac{D\varepsilon}{2\pi}}\left(\frac{\phi + 1}{\phi}\right) e^{-W^2} \tag{31}$$

and

$$V_{D2} = \kappa_2(-\infty)\ \sqrt{\frac{D\varepsilon}{2\pi}}\left(\phi + 1\right) e^{-W^2} \tag{32}$$

Thus, so far as the local flame structure is concerned, the features relevant to the turbulent flame calculation are determined by the local strain rate. Because of the simplicity of these analytical results, they will be employed in detailed calculations for the mixing zone and the fuel jet.

In many physical problems, the detailed distribution of chemical species plays a significant role, and, consequently, the simplification of the preceding calculation cannot be employed. But because of the effective separation of chemical aspects and turbulence, numerical calculations of even very complex flame structures is possible. To illustrate such a computation for a complex chemical reaction, we consider the reaction between hydrogen and atomic fluorine yielding hydrogen fluoride in the vibrational states v:

$$H_2 + F \rightarrow HF(v) + H \qquad v = 0, 1, 2, \text{ and } 3.$$

Because the vibrational population distribution produced by the reaction is partially inverted, the hydrogen fluoride can be caused to lase (in the

infrared) in a properly-designed laser cavity. In fact, H_2 - F and D_2 - F chemical lasers are among the most efficient. For this reason, the important rate coefficients have been determined to considerable accuracy and for the same reason, there is great interest in the turbulent combustion of these reactants. It is natural, therefore, to choose the H_2 - F flame for the illustration.

It is the chemical laser application as well that necessitates numerical calculation of the flame structure. To determine laser performance, it is not sufficient to know the H_2 and F consumption rates. In addition, the production of HF in the various vibrational levels is needed as is the subsequent depopulation rate of these levels by inter-molecular collisions. The accurate treatment of these processes and of the inter-diffusion of the many species involved is possible only in a numerical calculation.

For reasons irrelevant to the present discussion, the computations were carried out utilizing parallel streams of reactants that cause the development of the flame along the axis of the mixing zone. When the two streams have the same velocity U, the successive values of x can be considered as successive intervals in time defined by $t = x/U$. The results then become comparable to the time dependent diffusion flame with rapid kinetics discussed above. Correspondingly, when a pressure gradient is imposed upon the parallel stream to accelerate them in their direction of motion, the flame eventually reaches a structure that is independent of x and directly comparable with the steady, strained solution for rapid kinetics, also discussed above.

Consider then parallel, accelerating streams of nitrogen, one carrying the hydrogen and the other atomic fluorine. See Figure 2. At the initial station, $x = 0$, the pressure in both streams is 5 torr, the temperature is 500°K, and the velocity 10 cm/sec. In the upper stream, the fluorine and nitrogen mass fractions are 0.077 and 0.923, respectively; in the lower, the hydrogen and nitrogen mass fractions are 0.011 and 0.989, respectively. A constant strain is imposed on the flow by causing both streams to accelerate uniformly to 10^4 cm/sec in a distance of 6 inches. In the process, the pressure and temperature drop to 4.67 torr and 490°K, respectively.

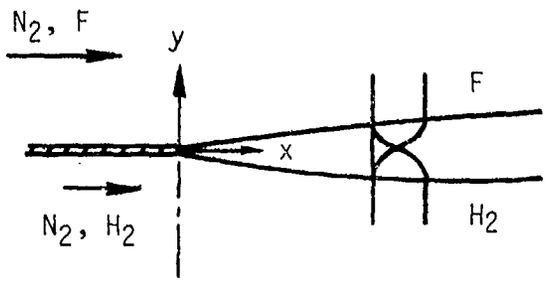

Figure 2. Strained Laminar Mixing Layer

The chemical reactions that are considered are described in detail in Reference 20. They may be summarized as follows. The reaction $H_2 + F \rightarrow HF(v) + H$ is unidirectional and produces vibrational populations in the following fractions: v = 0, 0.056; v = 1, 0.111; v = 2, 0.555; and v = 3, 0.278. The excited states are deactivated by collision with the other species present at prescribed efficiencies. In addition, there are V-V exchange collisions among the various levels of HF and with molecular hydrogen and nitrogen. The rate coefficients for all these molecular processes are given in Reference 20.

The multi-component diffusion coefficients are computed from temperature dependent binary coefficients under the assumption that the Lewis-Semenov number was constant. The temperature dependence of the species viscosities is accounted for by empirical fits to experimental data.

The system of equations describing this diffusing and chemically-reacting system was solved by a computer program that is a modification of the Blottner boundary layer code described in Reference 21. The original program has been modified so that it solves the laminar mixing layer equations and has subsequently been used in several investigations of the of the constant pressure hydrogen-fluorine flame.[22] A further modification was made to allow the treatment of the strained flame in the present study.

---

*The authors thank F. E. Fendell and D. Haflinger for making this modification and for obtaining the computer results that are presented.

Two sets of calculations were made: one with the complete chemical system outlined above and a second in which the HF was taken to be produced in a single (ground) state. This latter simplification was made so that an investigation of the effect of rate coefficient changes could be made more economically. These results are discussed first.

Figures 3 through 5 show the H_2, F and HF(0) y distributions at several downstream locations; that for Figure 3 being close to the initial stations. We observe first the evolution of the profiles into the fixed shape that the simple analysis, outlined at the beginning of this section, predicts for the strained flame. The profiles at x = 6.0 inches are virtually the same as those at x = 0.126 inch. This asymtotic state is attained even though neither the density nor the velocity are constant in the reaction zone. The density is reduced as the heat of reaction increases the temperature and then this lighter gas accelerates more than the free stream under the imposed pressure gradients.

The next point of interest in these results has to do with the chemical reaction rate relative to diffusion rate. We note that even for x locations as close as 0.126 inch to the origin, there is little interpenetration of hydrogen and fluorine. This observation suggests that the assumption made in the earlier analysis that the reaction rate is infinite may be a good approximation for the present condition. Additional evidence that this is the case was obtained by repeating the computation with the reaction rate coefficient increased by a factor ten. Comparison of Figure 6, given by the computation with Figure 5, shows only a minor increase in the amount of HF that has been formed, a result implying that diffusion to the flame surface is the rate-limiting process.

Vibrational state distributions for the run with the full hydrogen-fluorine chemistry are given in Figure 7 through 10. We see that the vibrational population total inversion which exists near the origin, $x = 10^{-6}$ inches, has, under the action of the deactivating collisions, nearly disappeared at $x = 4.4 \cdot 10^{-5}$ inches. (The inflection in the HF(v) distribution at the very low concentrations comes from computation errors and may be ignored.)

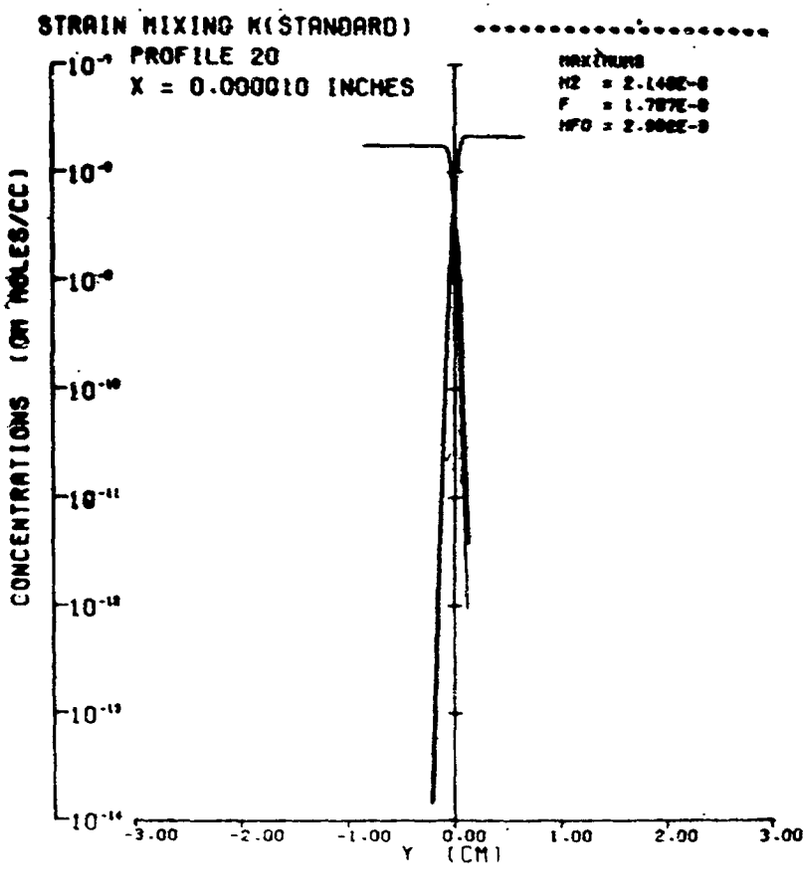

Figure 3. H_2, F, and HF Distributions in Strained Laminar H_2-F Flame at x = 10^{-5} Inches.

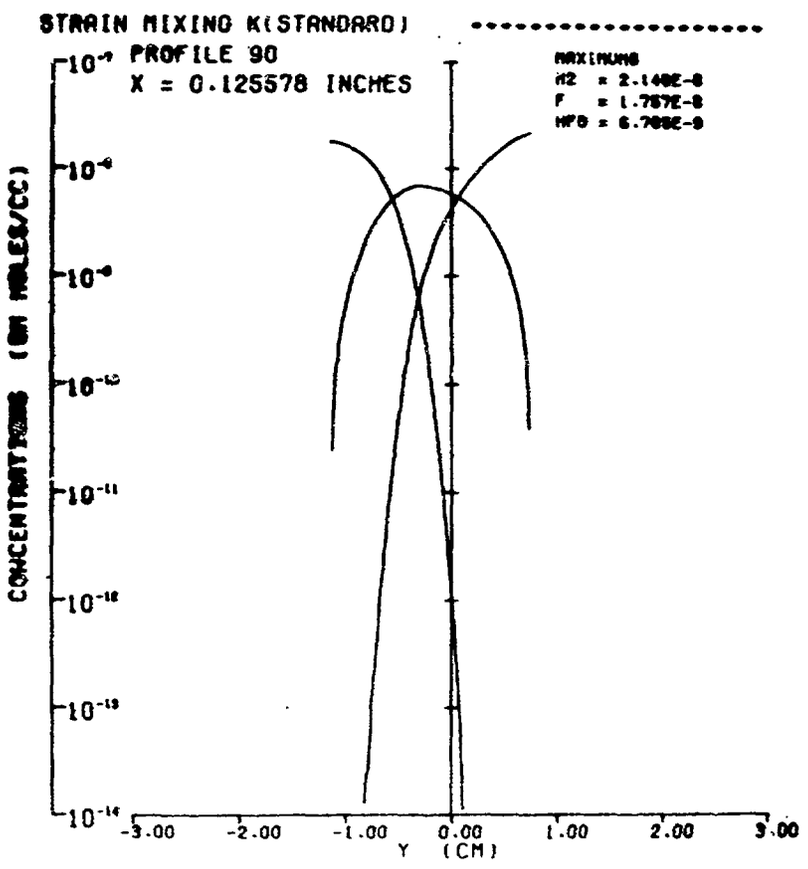

Figure 4. H_2, F, and HF Distributions in Strained Laminar H_2-F Flame at x = 0.126 Inches.

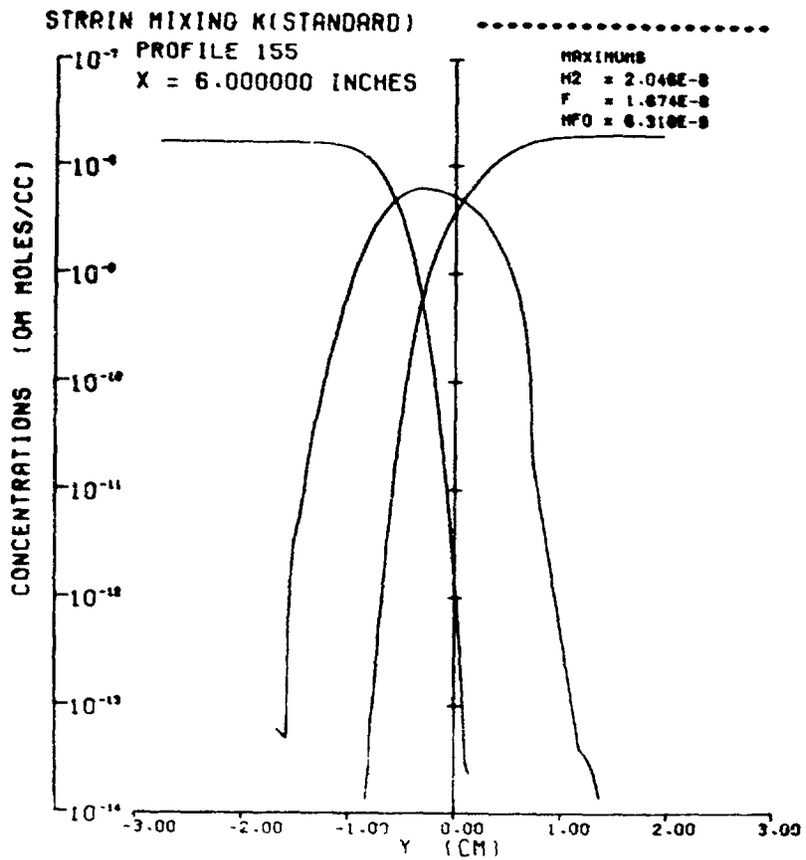

Figure 5. H_2, F, and HF Distributions in Strained Laminar H_2-F Flame at x = 6.0 Inches.

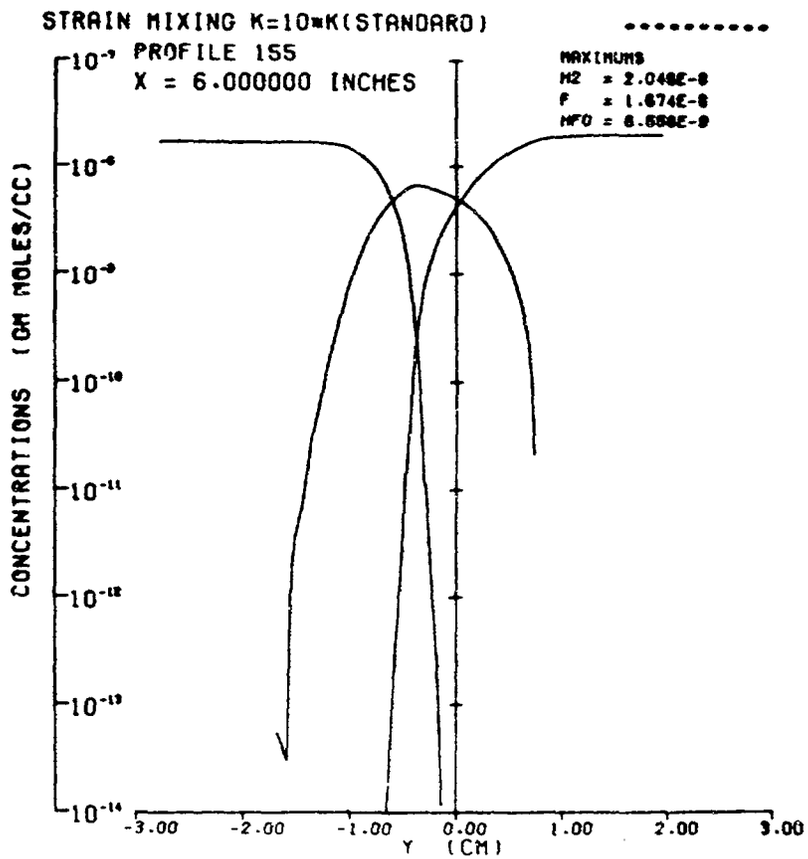

Figure 6. H_2, F, and HF Distributions in Strained Laminar H_2-F Flame at x = 6.0 Inches with Reaction Rate Coefficients Increased by Factor 10.

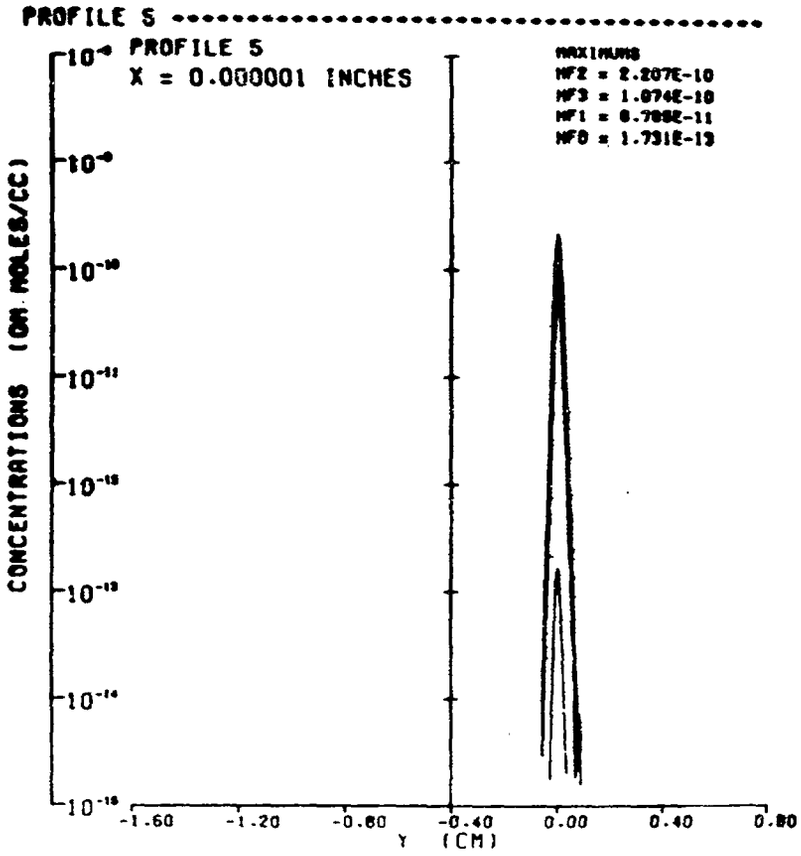

Figure 7. Ground and Excited HF Vibrational State Distributions in Strained Laminar H_2-F Flame at x = 10^{-6} Inches.

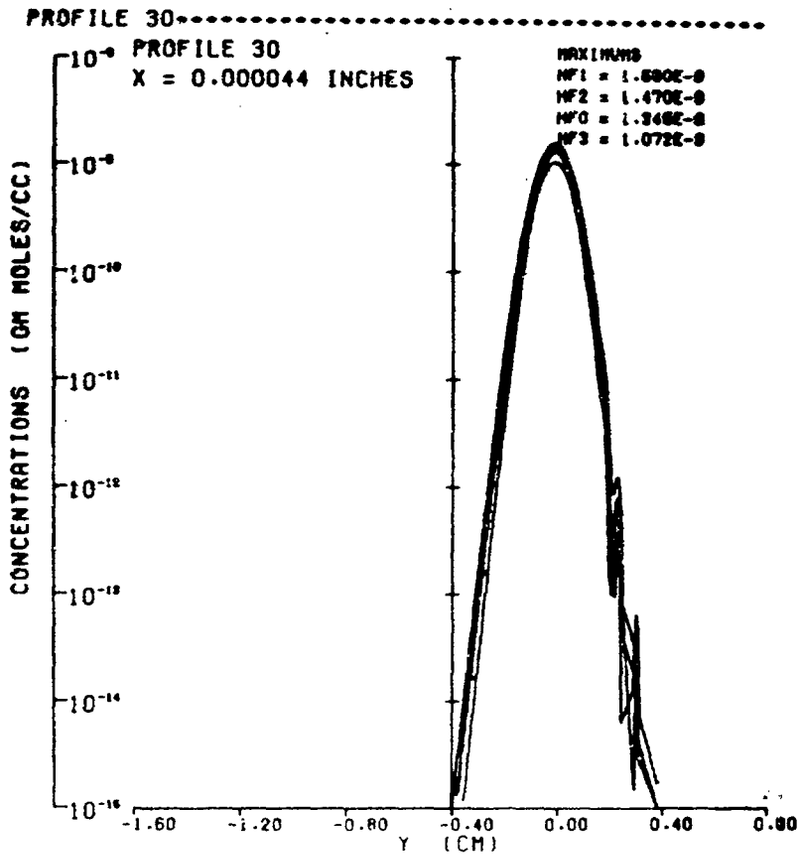

Figure 8. Ground and Excited HF Vibrational State Distributions in Strained Laminar H_2-F Flame at x = $4.4 \cdot 10^{-5}$ Inches.

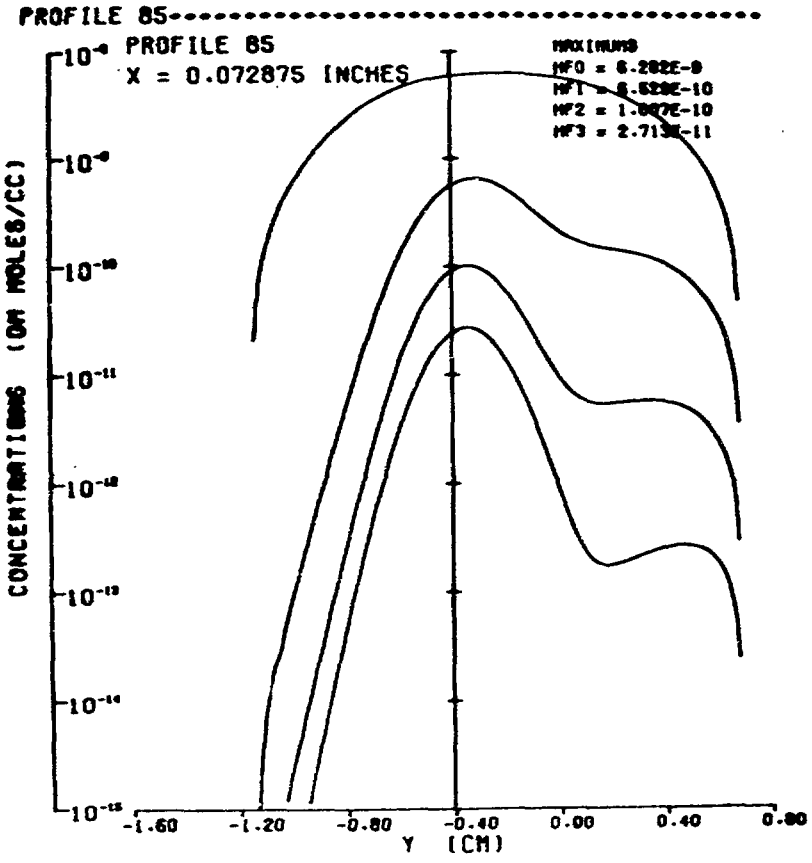

Figure 9. Ground and Excited HF Vibrational State Distributions in Strained Laminar H_2-F Flame at x = 7.29 · 10^{-2} Inches.

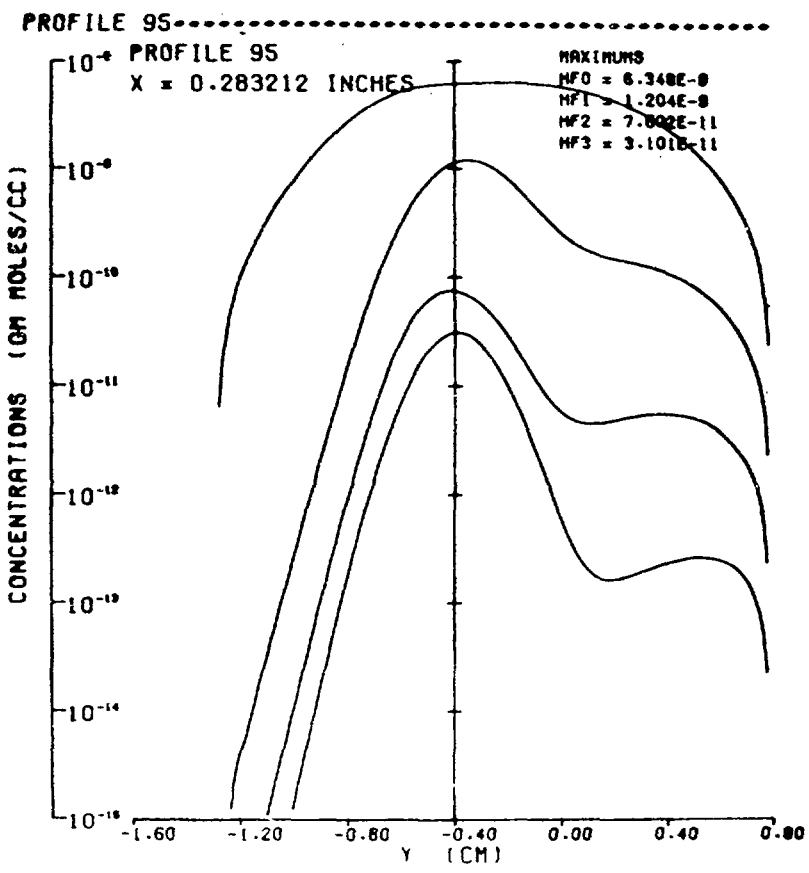

Figure 10. Ground and Excited HF Vibrational State Distributions in Strained Laminar H_2-F Flame at x = 0.28 Inches.

Comparison of Figures 9 and 10 indicates that, in this case, also the imposed constant strain rate has formed a flame whose width is constant and within which the state distributions are nearly constant. This result is perhaps somewhat unexpected in that the deactivation processes are distributed throughout the diffusion zone and, thus, the conditions of the chemical reaction are quite different from those in the simple analysis that lead to the constant state.

These results would be incorporated in the coherent flame model by determining the fuel and oxidizer consumption rates from the numerical solution. The state of the fluid within the turbulent flame zone would then be fixed by knowledge of the flame surface per unit volume, determined from the model, and the distribution within the flame. For all axial locations except those very close to the origin, the constant state strained distributions would be the appropriate ones. It appears, in fact, that in most applications, the strain-dominated flame solutions would be used.

In both the analysis and the numerical calculations just described, the assumption is made that no products are present when the flame begins. It is clear, however, that in those regions of the turbulent zone where flame shortening occurs, products are left behind which may influence the subsequent reaction. They may, for instance, separate volumes of fresh reactant and thereby reduce the reaction rate. The model has not yet been modified to account for such effects, but some indication of their significance may be obtained from the following idealization. Consider, as an initial condition, the situation sketched in Figure 11, meant to represent

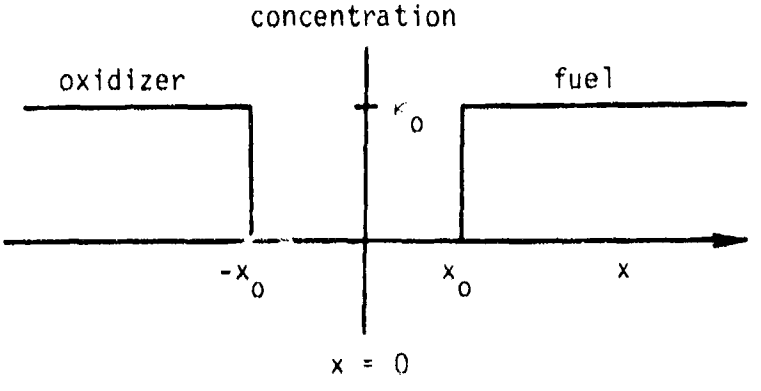

Figure 11. Initial Distribution of Reactants Separated by Product

fuel and oxidizer separated by an inert product layer 2 x_o thick. With the simplifying assumptions that the stoichiometric ratio is unity, the fuel and oxidizer concentrations are equal, the rate is infinite, and the density is constant, the reaction is confined to the plane x = 0 and the reactant concentrations there are held at zero for t > 0. The fuel concentration distribution satisfying the time-dependent diffusion equation with these boundary and initial conditions is:

$$\kappa_1 = \frac{\kappa_1(\infty)}{2\sqrt{\pi Dt}} \int_{x_o}^{\infty} \left[e^{-\frac{(x-x')^2}{4Dt}} - e^{-\frac{(x+x')^2}{4Dt}} \right] dx'$$

which can be written

$$\kappa_1 = \frac{\kappa_1(\infty)}{\sqrt{\pi}} \int_{x_o - x/2\sqrt{Dt}}^{x_o + x/2\sqrt{Dt}} e^{-z^2} dz$$

A similar expression applies, of course, to the oxidizer. From these solutions, the reactant flux to the flame sheet is found to be

$$\text{flux} = \rho D \left.\frac{\partial \kappa}{\partial x}\right|_{x=0} = \frac{\rho D \, \kappa_1(\infty)}{\sqrt{\pi Dt}} e^{-\frac{x_o^2}{4Dt}}$$

from which it is seen that the consumption rates differ from those of the classical case by the factor exp $(-x_o^2/4Dt)$. This result makes it clear that when large masses of product are interposed between the reactants, the diffusion flame structure may be strongly altered.

4. REACTION IN A TURBULENT MIXING ZONE

Consider the turbulent mixing and reaction of two parallel streams, the upper with undisturbed velocity U_1, fuel mass fraction $\kappa_1(\infty)$ and diluent mass fraction $\kappa_4(\infty) \equiv 1 - \kappa_1(\infty)$, the lower with undisturbed velocity U_2, oxidizer mass fraction $\kappa_2(-\infty)$ and diluent mass fraction $\kappa_4(-\infty) \equiv 1 - \kappa_2(-\infty)$. The problem is two-dimensional, steady, and will be treated under the boundary layer approximation. If we assume further that the molecular weights are nearly equal and that the molecularity of the reaction and heat evolved are small enough to produce negligible volumetric changes, then the coherent flame leads to the following formulation of the problem

$$\frac{\partial U}{\partial x} + \frac{\partial V}{\partial y} = 0 \tag{33}$$

$$U \frac{\partial U}{\partial x} + V \frac{\partial U}{\partial y} = \frac{\partial}{\partial y}\left(\frac{e}{\omega} \frac{\partial U}{\partial y}\right) \tag{34}$$

$$U \frac{\partial e}{\partial x} + V \frac{\partial e}{\partial y} = \frac{1}{2} \frac{\partial}{\partial y}\left(\frac{e}{\omega} \frac{\partial e}{\partial y}\right) + \alpha^* \left|\frac{\partial U}{\partial y}\right| e - \beta^* e \omega \tag{35}$$

$$U \frac{\partial \omega^2}{\partial x} + V \frac{\partial \omega^2}{\partial y} = \frac{1}{2} \frac{\partial}{\partial y}\left(\frac{e}{\omega} \frac{\partial \omega^2}{\partial y}\right) + \alpha \left|\frac{\partial U}{\partial y}\right| \omega^2 - \beta \omega^3 \tag{36}$$

In this problem, the magnitude of the mean rate-of-strain tensor and the magnitude of the velocity gradient tensor, as employed by Saffman, have the same value and appear in Equations 35 and 36. The turbulent exchange ratios, which relate the turbulent diffusion of energy or vorticity to the turbulent diffusion of momentum, have each been taken as 1/2, values found acceptable in Saffman's calculations.

The chemical reaction portion of the model will be formulated here utilizing the flame structure based upon very fast kinetics and dependence upon the local strain rate. According to this analysis, given in Section 3, the local volumetric consumption rates of fuel and oxidizer per unit flame area are $\kappa_1(\infty) \frac{1}{\phi} g(\phi) \sqrt{D\left|\partial U/\partial y\right|}$ and $\kappa_2(-\infty)\, g(\phi) \sqrt{D\left|\partial U/\partial y\right|}$ where again $|\partial U/\partial y|$

appears as the magnitude of the strain-rate tensor, a quantity denoted ε in Section 3 and $g(\phi) \equiv (1 + \phi) \exp(-W^2)$. Then the conservation equations for the fuel and oxidizer are

$$U \frac{\partial \kappa_1}{\partial x} + V \frac{\partial \kappa_1}{\partial y} = \frac{\partial}{\partial y}\left(\frac{e}{\omega} \frac{\partial \kappa_1}{\partial y}\right) - \kappa_1(\infty) \frac{1}{\phi} g(\phi) \sqrt{D\left|\frac{\partial U}{\partial y}\right|}\ \Sigma \tag{37}$$

$$U \frac{\partial \kappa_2}{\partial x} + V \frac{\partial \kappa_2}{\partial y} = \frac{\partial}{\partial y}\left(\frac{e}{\omega} \frac{\partial \kappa_2}{\partial y}\right) - \kappa_2(-\infty)\ g(\phi) \sqrt{D\left|\frac{\partial U}{\partial y}\right|}\ \Sigma \tag{38}$$

For the mass fractions of the product and inert diluent, we have similarly

$$U \frac{\partial \kappa_3}{\partial x} + V \frac{\partial \kappa_3}{\partial y} = \frac{\partial}{\partial y}\ \frac{e}{\omega} \frac{\partial \kappa_3}{\partial y}\ + \left[\frac{1}{\phi} \kappa_1(\phi) + \kappa_2(-\phi)\right] g(\phi) \sqrt{D\left|\frac{\partial U}{\partial y}\right|}\ \Sigma \tag{39}$$

$$U \frac{\partial \kappa_4}{\partial x} + V \frac{\partial \kappa_4}{\partial y} = \frac{\partial}{\partial y}\left(\frac{e}{\omega} \frac{\partial \kappa_4}{\partial y}\right) \tag{40}$$

Because of our assumptions regarding the nearly identical molecular weights of the gasses, the inert diluent is indistinguishable from other components and, hence, κ_4 may be grouped with any of the other constituents. The only alteration will be to define

$$\bar{\kappa}_1 = \left[1 + \frac{\kappa_4(\infty)}{\kappa_1(\infty)}\right] \kappa_1 \equiv \frac{\kappa_1}{\kappa_1(\infty)}\ ,\ \bar{\kappa}_2 = \left[1 + \frac{\kappa_4(-\infty)}{\kappa_2(-\infty)}\right] \kappa_2 \equiv \frac{\kappa_2}{\kappa_2(-\infty)}$$

and $\bar{\kappa}_3$ so as to satisfy the relation $\bar{\kappa}_1 + \bar{\kappa}_2 + \bar{\kappa}_3 = 1$. This general relation permits us to ignore Equation 39 and to rewrite 37 and 38

$$U \frac{\partial \bar{\kappa}_1}{\partial x} + V \frac{\partial \bar{\kappa}_1}{\partial y} = \frac{\partial}{\partial y}\left(\frac{e}{\omega} \frac{\partial \bar{\kappa}_1}{\partial y}\right) - \frac{1}{\phi} g(\phi) \sqrt{D\left|\frac{\partial U}{\partial y}\right|}\ \Sigma \tag{41}$$

$$U \frac{\partial \bar{\kappa}_2}{\partial x} + V \frac{\partial \bar{\kappa}_2}{\partial y} = \frac{\partial}{\partial y}\left(\frac{e}{\omega} \frac{\partial \bar{\kappa}_2}{\partial y}\right) - g(\phi) \sqrt{D\left|\frac{\partial U}{\partial y}\right|}\ \Sigma \tag{42}$$

Finally, the flame surface density equation is

$$U \frac{\partial \Sigma}{\partial x} + V \frac{\partial \Sigma}{\partial y} = \frac{\partial}{\partial y}\left(\frac{e}{\omega} \frac{\partial \Sigma}{\partial y}\right) + \alpha \left|\frac{\partial U}{\partial y}\right| \Sigma$$

$$- \lambda \frac{1}{\phi} g(\phi) \sqrt{D\left|\frac{\partial U}{\partial y}\right|}\ \Sigma^2/\bar{\kappa}_1 - \lambda\, g(\phi) \sqrt{D\left|\frac{\partial U}{\partial y}\right|}\ \Sigma^2/\bar{\kappa}_2 \tag{43}$$

Here we have used the same universal constant α in representing the flame surface stretching as was used in representing the vortex stretching in Equation 36. Note further that we have introduced only one additional universal constant, λ, in the flame shortening terms. The quadratic nature of the shortening terms allows any universal multiplier to be abosrbed in the definition of Σ itself; hence, only one additional constant is necessary.

Now because of our assumption of small density changes, the fluid mechanical problem is uncoupled from the flame structure, and a similarity solution for the turbulent mixing zone may be obtained in the same manner as given by Saffman. Then introducing $\xi \equiv x$, $\eta = y/x$ and defining a stream function

$$\psi = U_* \xi F(\eta) \tag{44}$$

where

$$U_* = \frac{1}{2}(U_1 + U_2) \tag{45}$$

the velocity components become

$$\begin{aligned} U &= U_* F'(\eta) \\ V &= U_* (\eta F' - F) \end{aligned} \tag{46}$$

Through dimensional considerations, it is appropriate to write the vorticity and the energy densities as

$$\omega = U_* \frac{1}{\xi} \Omega (\eta) \tag{47}$$

$$e = U_*^2 E (\eta) \tag{48}$$

where Ω and E are dimensionless functions of the similarity variable alone. With this representation, the turbulent diffusivity is

$$\mathcal{D} \equiv \frac{e}{\omega} = U_* \frac{E (\eta)}{\Omega (\eta)} \tag{49}$$

a result which allows the momentum Equation 34 to be written in similarity form

$$F F'' + \frac{d}{d\eta} \left(\frac{E}{\Omega} F'' \right) = 0 \tag{50}$$

With the similarity formalism already introduced, the vorticity and energy density equations, Equations 35 and 36, reduce to the following ordinary differential equations

$$-2\Omega \frac{d}{d\eta} (F\Omega) = \frac{d}{d\eta} (E\Omega') + \alpha F'' \Omega^2 - \beta \Omega^3 \tag{51}$$

and

$$-F E' = \frac{1}{2} \frac{d}{d\eta} \left(\frac{EE'}{\Omega} \right) + \alpha^* F''E - \beta^* \Omega E \tag{52}$$

Equations 50, 51, and 52 correspond to those given by Saffman for the mixing zone problem.

Turing now to the equations related to the flame and combustion problem, it is not obvious that they permit a corresponding similarity representation. The peculiar term that occurs in Equations 41, 42, and 43 is $\sqrt{D|\partial U/\partial y|}$ which we may write in terms of the similarity variables as

$$\sqrt{D\left|\frac{\partial U}{\partial y}\right|} = \sqrt{D\,\frac{1}{\xi}\left|\frac{\partial}{\partial \eta}\,(U_* F')\right|} = U_* \sqrt{\frac{D}{U_*\xi}\,|F''(\eta)|} \tag{53}$$

Then the formal representation of the flame structure, Equations 41 through 43, in the similarity variables of the fluid mechanical problem gives

$$F' \frac{\partial \bar{\kappa}_1}{\partial \xi} - \frac{1}{\xi} F \frac{\partial \bar{\kappa}_1}{\partial \eta} = \frac{1}{\xi} \frac{\partial}{\partial \eta}\left\{\frac{E}{\Omega}\frac{\partial \bar{\kappa}_1}{\partial \eta}\right\} - \frac{1}{\phi}\, g(\phi) \sqrt{\frac{D}{U_*\xi}\,|F''|}\;\Sigma \tag{54}$$

$$F' \frac{\partial \bar{\kappa}_2}{\partial \xi} - \frac{1}{\xi} F \frac{\partial \bar{\kappa}_2}{\partial \eta} = \frac{1}{\xi} \frac{\partial}{\partial \eta}\left\{\frac{E}{\Omega}\frac{\partial \bar{\kappa}_2}{\partial \eta}\right\} - g(\phi) \sqrt{\frac{D}{U^*\xi}\,|F''|}\;\Sigma \tag{55}$$

$$F' \frac{\partial \Sigma}{\partial \xi} - \frac{1}{\xi} F \frac{\partial \Sigma}{\partial \eta} = \frac{1}{\xi} \frac{\mu}{\partial \eta}\left\{\frac{E}{\Omega}\frac{\partial \Sigma}{\partial \eta}\right\} + \alpha\,\frac{1}{\xi}\,|F''|\;\Sigma \tag{56}$$

$$- \lambda\,\frac{1}{\phi}\, g(\phi) \sqrt{\frac{D}{U^*\xi}\,|F''|}\;\;\frac{\Sigma^2}{\bar{\kappa}_1} - \lambda\, g(\phi) \sqrt{\frac{D}{U_*\xi}\,|F''|}\;\;\frac{\Sigma^2}{\bar{\kappa}_2}$$

By inspection of these results, it appears that for similarity $\bar{\kappa}_1$ and $\bar{\kappa}_2$ are independent of ξ and that Σ behaves as $\xi^{-1/2}$. Thus, we have

$$\bar{\kappa}_1(\eta):\;\; \bar{\kappa}_1(\infty) = 1 \;\;,\;\; \bar{\kappa}_1(-\infty) = 0 \tag{57}$$

$$\bar{\kappa}_2(\eta):\;\; \bar{\kappa}_2(\infty) = 0 \;\;,\;\; \bar{\kappa}_2(-\infty) = 1 \tag{58}$$

and the flame density is expressed as

$$\Sigma\,(\xi,\eta) = \frac{L(\eta)}{g(\phi)\,\sqrt{D\xi/U_*}} \tag{59}$$

Note the appearance in this expression and in Equations 54 through 55 of the dimensionless streamwise variable

$$\zeta = \frac{U_* \xi}{D} \tag{60}$$

which bears the same relation to the Reynolds number as the molecular diffusivity D does to the kinematic viscosity. Note, then, that the quantity $\sqrt{D\xi/U_*}$ has the dimension of a length and gives the flame surface density its dimension of a reciprocal length, the variable $L(\eta)$ being the dimensionless. Then, we use the new density variable

$$L(\eta): \quad L(\infty) = L(-\infty) = 0 \tag{61}$$

With these definitions, Equations 54 through 56 reduce to ordinary differential equations in $\bar{\kappa}_1(\eta)$, $\bar{\kappa}_2(\eta)$, and $L(\eta)$:

$$- F \bar{\kappa}_1' = \frac{d}{d\eta}\left(\frac{E}{\Omega} \bar{\kappa}_1'\right) - \frac{1}{\phi} \sqrt{|F''|}\, L \tag{62}$$

$$- F \bar{\kappa}_2' = \frac{d}{d\eta}\left(\frac{E}{\Omega} \bar{\kappa}_2'\right) - \sqrt{|F''|}\, L \tag{63}$$

$$- \frac{1}{2} F' L - F L' = \frac{d}{d\eta}\left(\frac{E}{\Omega} L'\right) + \alpha |F''| L - \lambda \frac{1}{\phi} \sqrt{|F''|}\, \frac{L^2}{\bar{\kappa}_1} - \lambda \sqrt{|F''|}\, \frac{L^2}{\bar{\kappa}_2} \tag{64}$$

In contrast to some formulations of turbulent mixing problems, the present one, because of its non-linear turbulent diffusivity, may produce a sharp boundary between the turbulent zone and the far field. This not unfamiliar situation was discussed in some detail by Saffman[18] in connection with the fluid dynamic solutions of several problems. The relevant point here is that, with the non-linear diffusivity employed, the edges in this case are sharp, lying at constant values of η, these values emerging as characteristic of the problem. With the value of 1/2 chosen as the exchange ratio in Equations 35 and 36, the appropriate boundary values for F, E, and Ω are

$$F(\eta_1) = \frac{U_1}{U_*}$$

$$F(\eta_2) = \frac{U_2}{U_*}$$

$$\Omega(\eta_1) = \Omega(\eta_2) = 0 \qquad (65)$$

$$E(\eta_1) = E'(\eta_1) = E(\eta_2) = E'(\eta_2) = 0$$

Subjecting the flame variables $\bar{\kappa}_1$, $\bar{\kappa}_2$, and L to a corresponding analysis, we find for the equations -- as formulated --

$$\bar{\kappa}_1(\eta_1) = \bar{\kappa}_1(\eta_2) = 0$$

$$\bar{\kappa}_2(\eta_1) = \bar{\kappa}_2(\eta_2) = 0 \qquad (66)$$

$$L(\eta_1) = L(\eta_2) = 0$$

Clearly, there exists a trivial solution $L(\eta) = 0$, and in this case, κ_1 and κ_2 simply become constituents that mix without chemical reaction. In fact, $\bar{\kappa}_1(\eta)$ and $\bar{\kappa}_2(\eta)$ are linear functions of $F'(\eta)$, but this is not the solution we seek.

Some properties of the solution can be obtained quite easily, for example the total fuel consumed per unit length of the mixing zone. This follows from integration of either Equation 41 or Equation 62 across the mixing layer. Working with Equation 41, we find

$$\int_{y_2}^{y_1} \frac{\partial}{\partial x}(U\,\bar{\kappa}_1)\,dy + \int_{y_2}^{y_1} \frac{\partial}{\partial y}(V\,\bar{\kappa}_1)\,dy = -\int_{y_2}^{y_1} \frac{1}{\phi}\,g(\phi)\,\sqrt{D\left|\frac{\partial U}{\partial y}\right|}\,\Sigma,\,dy$$

which, with appropriate substitution for the variables, leads to

$$\frac{d}{dx}\int_{y_2}^{y_1} U\,\bar{\kappa}_1\,dy = U_1\eta_1 - \frac{1}{\phi}U_*\int_{\eta_2}^{\eta_1}\sqrt{|F''|}\,L\,d\eta \tag{67}$$

This expresses the change with respect to x of fuel flux in the mixing zone, given by the integral on the left, as the difference between the flux of fuel in at the upper boundary and the fuel consumed by the chemical reaction. The striking result is that this rate is independent of distance along the mixing zone, in spite of the fact that all other physical quantities have some x-dependence.

Calculations by Milinazzo and Saffman[18] have provided a good basis for the formulation of an integral solution to the turbulent mixing zone which we carry through the flame zone problem as well. For this purpose, we approximate the stream functions

$$F(\eta) = \frac{\frac{U_2}{U_*}\eta_1 - \frac{U_1}{U_*}\eta_2}{\eta_1 - \eta_2}\eta + \frac{1}{2}\frac{\frac{U_1}{U_*} - \frac{U_2}{U_*}}{\eta_1 - \eta_2}\eta^2 \tag{68}$$

$$\Omega(\eta) = \Omega_o\,(\eta_1 - \eta)\,(\eta - \eta_2) \tag{69}$$

$$E(\eta) = E_o\,(\eta_1 - \eta)^2\,(\eta - \eta_2)^2 \tag{70}$$

in which η_1, η_2, Ω_o, and E_o appear as constants (functions of the problem parameters) to be determined by the integral relations. Using integrals of the energy and vorticity equations, together with integrals from 0-η_1 and from η_2-0 of the momentum equation, the problem reduces to an algebraic solution. The technique is familiar and straightforward, although algebraically tedious and the details will be omitted. For small values of $(U_1 - U_2)/U_*$, we find that

$$\eta_1 = -\eta_2 = 0.1125\left(\frac{U_1 - U_2}{\frac{1}{2}(U_1 + U_2)}\right)$$

$$E_o\left(\frac{U_1 - U_2}{\frac{1}{2}(U_1 + U_2)}\right) = \Omega_o = 153.64 \tag{71}$$

The values of η_1 for specific values of U_2/U_1 correspond very well with numerical results given by Milinazzo and Saffman.[18]

The integral method may also be applied to the species conservation equations and flame density equation, providing suitable representation for the profiles may be constructed. Those chosen were

$$\kappa_1 = f_1(\eta) + C_1\, g(\eta) \tag{72}$$

$$\kappa_2 = f_2(\eta) + C_2\, g(\eta) \tag{73}$$

$$L(\eta) = D\,(f_1 + C_1\, g)(f_2 + C_2\, g) \tag{74}$$

where the functions f_1, f_2, and g are

$$f_1 = \frac{\eta - \eta_2}{\eta_1 - \eta_2}\left\{1 - \left(\frac{\eta_1 - \eta}{\eta_1 - \eta_2}\right)^2 + \frac{(\eta_1 - \eta)(\eta - \eta_2)}{(\eta_1 - \eta_2)^2}\right\} \tag{75}$$

$$f_2 = \frac{\eta_1 - \eta}{\eta_1 - \eta_2}\left\{1 - \left(\frac{\eta - \eta}{\eta_1 - \eta_2}\right)^2 + \frac{(\eta_1 - \eta)(\eta - \eta_2)}{(\eta_1 - \eta_2)^2}\right\} \tag{76}$$

$$g = \frac{(\eta_1 - \eta)^2\,(\eta - \eta_2)^2}{(\eta_1 - \eta_2)^4} \tag{77}$$

$$C_1 = C_2 = \frac{-3.857}{\frac{1}{2}(1 + \phi) + 0.815\,\lambda}$$

$$D = 0.4286/\lambda \tag{78}$$

If we utilize the integral technique to evaluate the fuel consumption rate in the mixing zone, as expressed by Equation 67, we find that approximately

$$\frac{d}{dx}\int_{y_2}^{y_1} U\,\bar{\kappa}_1\,dy \tag{79}$$

$$= |U_1 - U_2| \left\{ 0.225\,\frac{U_1}{U_1 + U_2} - \frac{0.037}{\lambda\phi}\left(1 - \frac{1}{\frac{1}{2}(1 + \phi) + 0.815\,\lambda}\right)\right\}$$

valid for limited variations of ϕ from unity. To the same approximation, the ratio of fuel consumption to fuel inflow is

$$0.164\left(1 + \frac{U_2}{U_1}\right)\frac{1}{\lambda\phi}\left(1 - \frac{1}{\frac{1}{2}(1 + \phi) + 0.815\,\lambda}\right) \tag{80}$$

5. TURBULENT FUEL JET

The fuel jet problem utilizes the same general equations for the fluid dynamics as employed for the mixing zone, Section 4, and because we approximate the jet by a two-dimensional momentum source, the solution has the familiar similarity property. The similarity, again, rests on the assumption that the heat addition is small so that the fluid mechanical and combustion problems separate. The combustion part of the problem does not have a similarity solution, however, simply because there is a finite amount of fuel injected and this is eventually consumed, so that the chemical reaction ceases. Moreover, the classical "point" jet similarity solution carries an initially zero mass flux while the fuel jet problem requires a fixed flux of fuel to be injected at the origin. This difficulty is resolved in the familiar manner by displacing the effective origin to an appropriate point downstream of the momentum source.

Because the combustion solution is ron-similar, the differential equations for the chemical species and the flame surface density do not reduce to ordinary differential equations, but become partial differential equations in terms of the fluid dynamic similarity variables. Simplification of the resulting problem is achieved by the familiar procedure of constructing a linear combination of the various mass fractions in which specific atom concentrations are conserved and, hence, satisfy a homogeneous differential equation. In the present case, it proves possible to develop such a combination of fuel and oxidizer mass fractions that is equal to the similarity velocity distribution. The mathematical problem then reduces to a pair of partial differential equations, one linear and one non-linear, with an algebraic integral which allows determination of the individual species mass fractions.

The similarity variables for the two-dimensional jet follow from the observations: i) that there is no natural length and, hence, the jet should spread linearly along lines $\eta \equiv x/y$ = constant, and ii) that the momentum injected by the jet is conserved so that the integral $\int u^2\, dy$ over the jet is constant. But since the jet width increases directly with x, the velocity distribution must vary as $x^{-1/2}$. It also follows that the flow in the jet varies as $x^{1/2}$, so that the injected mass flow is zero, the point that prompted the earlier observation about fuel flow.

The appropriate variables are then

$$\xi = x$$
$$\eta = y/x \tag{81}$$

and if we denote the momentum efflux from the jet, per unit depth of the x-y plane, as $\rho\mu$, where ρ is the constant density of the fluid, then it is appropriate to write the stream function

$$\psi = \sqrt{\mu\xi}\, F(\eta) \tag{82}$$

For the similarity to hold, it is clear from Equation 7 that $\frac{e}{\omega} \equiv \mathcal{D} \sim \xi^{1/2}$, and from Equation 8 that $\omega \sim \xi^{-3/2}$. Therefore, it is appropriate to write

$$\omega = \frac{\mu^{1/2}}{\xi^{3/2}}\, \Omega(\eta) \tag{83}$$

$$e = \frac{\mu}{\xi}\, E(\eta) \tag{84}$$

with $\Omega(\eta)$ and $E(\eta)$ dimensionless. Under these definitions, the velocity components are

$$U = \sqrt{\frac{\mu}{\xi}}\, F' \tag{85}$$

$$V = \sqrt{\frac{\mu}{\xi}} \left[\frac{1}{2} F - \eta F'\right] \tag{86}$$

and Equation 6 becomes

$$-\frac{1}{2}(F')^2 - \frac{1}{2} F F' = \frac{1}{2} \frac{d}{d\eta}\left(\frac{E}{\Omega} F''\right) \tag{87}$$

The momentum equation may be integrated directly to give

$$\frac{1}{2} F F' + \frac{E}{\Omega} F'' = 0$$

where the constant of integration vanishes because of the conditions on F' and E/Ω at the edge of the jet. Equation 7 reduces to the form

$$- F' E - \frac{1}{2} F E' = \frac{1}{2} \frac{d}{d\eta} \left\{ \frac{E}{\Omega} E' \right\} + \alpha^* |F''| E - E\Omega \tag{88}$$

where, following Saffman's choice, we have taken $\beta^* = 1$. We note further by the boundary conditions and symmetry of the problem, $|F''| = - F''$ for $\eta \geq 0$ in which region the calculation will be carried out. Finally, Equation 8 becomes

$$- 3F' \Omega^2 - F \Omega \Omega' = \frac{d}{d\eta} (E \Omega') + \alpha |F''| \Omega^2 - \beta \Omega^3 \tag{89}$$

The conditions on the dependent variables are that, at the edge η_1 of the jet, $F'(\eta_1) = \Omega(\eta_1) = E'(\eta_1) = 0$, while on the symmetry axis, $F(0) = E'(0) = \Omega'(0) = 0$. In addition, the momentum μ per unit mass is

$$2 \int_0^{\eta_1} \left(\sqrt{\frac{\mu}{\xi}} F' \right)^2 dy = \mu$$

from which it follows that

$$\int_0^{\eta_1} (F')^2 \, d\eta = \frac{1}{2} \tag{90}$$

In treating the chemical composition and flame density, we make corresponding assumptions that were made for the mixing layer concerning molecular weights of the constituent and the possibility of grouping an inert diluent with any of the other constituents. Thus, we deal with only three species that satisfy equations

$$U \frac{\partial \bar{\kappa}_1}{\partial x} + V \frac{\partial \bar{\kappa}_1}{\partial y} = \frac{\partial}{\partial y}\left(\frac{e}{\omega} \frac{\partial \bar{\kappa}_1}{\partial y}\right) - \frac{1}{\phi} g(\phi) \sqrt{D\left|\frac{\partial U}{\partial y}\right|}\ \Sigma \tag{91}$$

$$U \frac{\partial \bar{\kappa}_2}{\partial x} + V \frac{\partial \bar{\kappa}_2}{\partial y} = \frac{\partial}{\partial y}\left(\frac{e}{\omega} \frac{\partial \bar{\kappa}_2}{\partial y}\right) - g(\phi) \sqrt{D\left|\frac{\partial U}{\partial y}\right|}\ \Sigma \tag{92}$$

$$U \frac{\partial \bar{\kappa}_3}{\partial x} + V \frac{\partial \bar{\kappa}_3}{\partial y} = \frac{\partial}{\partial y}\left(\frac{e}{\omega} \frac{\partial \bar{\kappa}_3}{\partial y}\right) + \left(1 + \frac{1}{\phi}\right) g(\phi) \sqrt{D\left|\frac{\partial U}{\partial y}\right|}\ \Sigma \tag{93}$$

Now by virtue of the linearity of these equations in their respective concentrations and the fact that the consumption terms differ by only multiplicative constants, it is possible to write linear combinations of the mass fractions that are conserved. The obvious one, which we have utilized in the last example, is

$$\bar{\kappa}_1 + \bar{\kappa}_2 + \bar{\kappa}_3 = 1 \tag{94}$$

where the normalization is included in the definition of mass fraction. A second linear combination, of use to us in the present example, is

$$J = \bar{\kappa}_1 + \frac{1}{1 + \phi} \bar{\kappa}_3 \tag{95}$$

which satisfies the homogeneous equation

$$U \frac{\partial J}{\partial x} + V \frac{\partial J}{\partial y} = \frac{\partial}{\partial y}\left(\frac{e}{\omega} \frac{\partial J}{\partial y}\right) \tag{96}$$

and vanishes for large values of y, outside the jet. Therefore, because it satisfies the same equations and the same remote conditions as U(x,y), it is proportional to this function and the constant of porportionality must be given by an integral condition, similar to the momentum integral, Equation 90, for the jet itself.

This condition can be determined by stipulating that the jet initially injects a volume flow rate γ_1 of fuel which implies that the entire injected flow rate of fuel plus diluent is $\gamma_1 [1 + \kappa_4(0)/\kappa_1(0)]$. Far from the point

of injection, where the fuel is entirely reacted to combustion products, the jet will carry a flow rate of combustion products

$$\gamma_1 \left[1 + \frac{\kappa_4(\infty)}{\kappa_1(\infty)}\right] + \frac{\gamma_1}{f}\left[1 + \frac{\kappa_4(\infty)}{\kappa_2(\infty)}\right] \tag{97}$$

in which the injected flow has been augmented by the chemically correct amount of the ambient fluid to react the fuel in the stoichiometric ratio. Calling

$$\gamma \equiv \gamma_1 \left[1 + \frac{\kappa_4(0)}{\kappa_1(0)}\right] \tag{98}$$

expression 97 becomes

$$\gamma \left[1 + \frac{1}{f}\left(\frac{\kappa_2(\infty) + \kappa_4(\infty)}{\kappa_1(0) + \kappa_4(0)}\right)\left(\frac{\kappa_1(0)}{\kappa_2(\infty)}\right)\right] = \gamma(1 + \phi) \tag{99}$$

Thus the integral condition on the reaction products is, where the reaction is complete,

$$\lim_{x \to \infty} 2 \int_0^{y_1} U \bar{\kappa}_3 \, dy = \gamma(1 + \phi) \tag{100}$$

But, because $\kappa_1 \to 0$ for large x, indicating that the fuel is eventually reacted, Equation 95 gives

$$\lim_{x \to \infty} J = \frac{1}{1 + \phi} \lim_{x \to \infty} \bar{\kappa}_3$$

so that

$$\lim_{x \to \infty} 2 \int_0^{y_1} U J \, dy = \gamma \tag{101}$$

To express this condition, it has been necessary to introduce a volume flow rate γ of material that initially constitutes the jet which, in turn,

must carry the momentum μ. This is clearly not admissible in the theory of the point jet, for which $\gamma = 0$, because between the flow rate and momentum flux, we may define a length γ^2/μ and a velocity μ/γ that characterize a jet of finite dimensions. The appropriate viewpoint, however, is similar to the description of a finite jet by means of a point jet with a displaced origin, and shares with that approximation the difficulty that some early portion of the jet structure is described inaccurately.

Now because the function $J(x,y)$ is proportional to the velocity $U(x,y)$, it may be written in similarity coordinates

$$J = \sqrt{\frac{d}{\xi}}\ F'(\eta) \tag{102}$$

where d is an unknown length. Substituting this expression in Equation 101 gives

$$\lim_{\xi\to\infty} 2\int_0^{y_1}\left(\sqrt{\frac{\mu}{\xi}}\,F'\right)\left(\sqrt{\frac{d}{\xi}}\,F'\right)dy = \lim_{\xi\to\infty}\ \sqrt{\mu d}\int_0^{\eta_1}(F')^2\,d\eta = \gamma \tag{103}$$

But the integral is independent of ξ and holds for all ξ so that the normalization of the momentum integral, Equation 90, permits determination of the unknown length scale,

$$d = \frac{\gamma^2}{\mu} \tag{104}$$

which we have defined earlier as the effective height of the jet discharge.

The explicit solution for J that we have obtained permits us, using Equations 94 and 95, to write the oxidizer mass fraction in the form

$$\bar{\kappa}_2 = 1 - \bar{\kappa}_1 - (1+\phi)(J - \bar{\kappa}_1) = 1 + \phi\ \kappa_1 - (1+\phi)\ J$$

and therefore

$$\bar{\kappa}_2 = 1 + \phi\ \bar{\kappa}_1 - (1+\phi)\ \sqrt{\frac{d}{\xi}}\,F'(\eta) \tag{105}$$

This algebraic integral, together with Equation 94, makes it necessary to determine only two unknowns, $\kappa_1(\xi,\eta)$ and $\Sigma(\xi,\eta)$, by the solution of differential equations.

To complete the formulation of the jet problem, we shall consider the expressions for fuel conservation, Equation 91, and the flame surface density, Equation 2, the latter written in the form

$$U \frac{\partial \Sigma}{\partial x} + V \frac{\partial \Sigma}{\partial y} = \frac{\partial}{\partial y}\left(\frac{e}{\omega} \frac{\partial \Sigma}{\partial y}\right) + \alpha \left|\frac{\partial U}{\partial y}\right| \Sigma - \lambda\, g(\phi) \sqrt{D\left|\frac{\partial U}{\partial y}\right|} \frac{\Sigma^2}{\bar{\kappa}_1 \bar{\kappa}_2} \qquad (106)$$

This form of the flame density equation differs slightly from that we employed previously, in the form of the flame shortening terms. Here, the two terms are replaced by a single one that reproduces the general physical idea and preserves the important behavior of the term at $\bar{\kappa}_1 = 0$ and at $\bar{\kappa}_2 = 0$, since the two never vanish simultaneously.

It remains to write Equations 91 and 106 in similarity variables and to make the appropriate choices for the detailed representations for $\bar{\kappa}_1$ and Σ. Note that if there were no reactant consumption terms in Equation 91 for the fuel mass fraction, the quantity $\bar{\kappa}_1$ would also be proportional to the velocity and to emphasize this fact, we write

$$\bar{\kappa}_1 = \sqrt{\frac{d}{\xi}}\, k_1(\xi,\eta) \qquad (107)$$

remembering that in the absence of combustion, $k_1(\xi,\eta) = F'(\eta)$. Furthermore, it will prove convenient to define a new variable (cf. Equation 59) related to the flame density

$$\frac{1}{d}\, g(\phi) \left(\frac{\xi}{d}\right)^{5/4} \sqrt{\frac{D}{\gamma}}\; \Sigma(\xi,\eta) = L(\xi,\eta) \qquad (108)$$

where it is particularly to be noted that a dimensionless physical parameter has been constructed of the molecular diffusivity and the volume flow γ per

unit depth. It is then a matter of a straightforward reduction to show that $k_1(\xi,\eta)$ and $L(\xi,\eta)$ satisfies the partial differential equations

$$F' \xi \frac{\partial k_1}{\partial \xi} - \frac{1}{2} F' k_1 - \frac{1}{2} F \frac{\partial k_1}{\partial \eta} = \frac{\partial}{\partial \eta}\left[\frac{E}{\Omega}\frac{\partial k_1}{\partial \eta}\right] - \frac{1}{\phi}\sqrt{|F''|}\, L \tag{109}$$

and

$$F' \xi \frac{\partial L}{\partial \xi} - \frac{5}{4} F'L - \alpha|F''|L - \frac{1}{2} F \frac{\partial L}{\partial \eta} = \frac{\partial}{\partial \eta}\left(\frac{E}{\Omega}\frac{\partial L}{\partial \eta}\right) - \lambda \sqrt{|F''|}\,\frac{L^2}{k_1 \bar{\kappa}_2} \tag{110}$$

where now, from Equation 105,

$$\bar{\kappa}_2 = 1 - \sqrt{\frac{d}{\xi}}\left[F' + \phi\left(F' - k_1(\xi,\eta)\right)\right] \tag{111}$$

For use in some of the calculations that follow, and because of their intrinsic value, the fuel and flame density equations may be integrated across the jet to give the resulting relations

$$\xi \frac{d}{d\xi}\int_{-\eta_1}^{\eta_1} F' k_1 \, d\eta = -\frac{1}{\phi}\int_{\eta_1}^{\eta} \sqrt{|F''|}\, L \, d\eta \tag{112}$$

and

$$\left(\xi \frac{d}{d\xi} - \frac{3}{4}\right)\int_{-\eta_1}^{\eta_1} F' L \, d\eta = \alpha \int_{-\eta_1}^{\eta_1} |F''|L \, d\eta - \lambda \int_{-\eta_1}^{\eta_1} \sqrt{|F''|}\,\frac{L^2}{k_1 \kappa_2}\, d\eta \tag{113}$$

The single term on the right-hand side of Equation 112 represents the integrated fuel consumption, while those terms on the right-hand side of Equation 113 represent, respectively, the flame surface growth by stretching and the flame shortening by mutual annihilation.

The problem of the turbulent jet has been treated numerically utilizing an integral technique and reasonable representations of the profiles. In chosing the general profiles to represent the vorticity and energy densities in the turbulence, numerical calculations done by Dr. F. Milinazzo, privately communicated to the authors, were very useful.

Again, omitting the tedious algebraic details that characterize an integral method, it was found that the velocity, vorticity, and energy distributions could be represented adequately as

$$F' = F'(0)\left(\frac{1-\delta^2}{4}\right)\left\{1+3\,(1-\delta^2)\right\} \tag{114}$$

$$\Omega = \Omega(0)\,(1-\delta^2) \tag{115}$$

$$E = E(0)\,\frac{(1-\delta^2)^2}{3}\left\{7-3\,(1-\delta^2)^2\right\} \tag{116}$$

where $F'(0)$, $\Omega(0)$, and $E(0)$ are the values of these variables on the symmetry axis and

$$\delta = \eta/\eta_1 \tag{117}$$

and their numerical values are

$$\begin{aligned} F'(0) &= 1.995 \\ \Omega(0) &= 3.570 \\ E(0) &= 0.724 \\ \eta_1 &= 0.290 \end{aligned} \tag{118}$$

As before, the values of the universal constants in the turbulence model were taken as $\alpha = 0.2$, $\alpha^* = 0.3$, and $\beta = 5/3$.

Proceeding to the combustion portion of the model, we wish to reduce the integral relations, Equations 112 and 113, to ordinary differential equations by the choice of fuel concentration and flame density profiles. The results are made more manageable by the separation of ξ and η dependence of these functions to the degree reasonable. With this aim in mind, we choose to represent

$$k_1(\xi,\eta) = k(\xi)\,F'(\eta) \tag{119}$$

which for $k(\xi) = 1$, yields an exact result in the absence of chemical reaction, and, consequently, we know in general that $k(\xi) \leq 1$. The fuel

mass fraction then becomes

$$\bar{\kappa}_1(\xi,\eta) = \sqrt{\frac{d}{\xi}}\, k(\xi)\, F'(\eta) \tag{120}$$

so that, for the physical bound that $\bar{\kappa}_1 \leq 1$ to hold, there is a lower limit on the value of ξ for which our representation is valid. Clearly this is

$$\left.\frac{\xi}{d}\right|_{min} = \left(F'(0)\right)^2 = 3.980 \tag{121}$$

and we shall consider this as the minimum value of ξ for which we can expect a reasonable representation of the jet flame.

The choice for the flame density representation will be

$$L(\xi,\eta) = \ell(\xi)\, k_1(\xi,\eta)\, \bar{\kappa}_2(\xi,\eta) \tag{122}$$

which has the obvious advantages not only of behaving correctly at the jet boundaries but in making the second integral on the right-hand side of Equation 113 more convenient to handle. Substituting the representations for $k_1(\xi,\eta)$ and $\bar{\kappa}_2(\xi,\eta)$, Equations 111 and 119, respectively, we write

$$L(\xi,\eta) = g(\xi)\, F' \left\{ 1 - \sqrt{\frac{d}{\xi}}\, F' \left[1 + \phi - \phi\, k(\xi) \right] \right\} \tag{123}$$

where $g(\xi)$, formally equal to $\ell(\xi)\, k(\xi)$, appears as the second unknown function. It is assumed in the representations of both $\bar{\kappa}_1(\xi,\eta)$ and $L(\xi,\eta)$ that $F'(\eta)$, where it occurs, is given by Equation 115 and, hence, known.

Again omitting much laborious detail and denoting $\sqrt{\xi/d} \equiv z$, the species concentration integral, Equation 112, may be written

$$z\, \frac{d}{dz}\, (\phi k) = -\, 3.0737 \left[1 - 1.676 \left(\frac{1 + \phi - \phi k}{z} \right) \right] \tag{124}$$

where it is convenient to use the group ϕk in the numerical calculations. Proceding in a similar manner, the integrated equation for the flame

density, Equation 113, becomes

$$z \frac{dg}{dz} = \frac{g}{M} \left\{ \frac{1}{2} (5M + 1.2295\ N - 2) + 3.0737\ Ng \left[- \frac{\phi\lambda}{\phi k} + 1.6755 \left(\frac{1}{z} \right) \right] \right\} \quad (125)$$

where

$$M = 1 - 1.6755 \left(\frac{1 + \phi - \phi k}{z} \right) \quad (126)$$

$$N = 1 - 1.4109 \left(\frac{1 + \phi - \phi k}{z} \right) \quad (127)$$

The numerical integration requires specification of the equivalence ratio ϕ and the initial value $k(z_o) = 1$. In addition, a value for the universal constant λ must be selected and the initial value $g(z_o)$ specified. One of the difficulties in our point jet approximation is that the initial development of the jet of finite cross section is not described correctly. Therefore, the present theory gives no description of the transition between the mixing zone-dominated portion and the fully-developed jet and, hence, provides no information concerning the flame density with which to initiate the jet calculation. It is possible to make an estimate for $g(z_o)$ from the results obtained in Section 4 for the flame structure of the mixing zone. While a matching procedure has not been carried out in detail for various values of ϕ, it appears that $0.1 < g(z_o) < 0.3$ is reasonable for non-extreme values of the equivalence ratio.

In the calculations that have been carried out, $g(z_o)$ has generally been taken as 0.2, and the effects of variations from this value have been explored only to a limited extent. The item of principle interest in the calculation is the variation of the fuel concentration along the jet axis. It is this quantity that is frequently measured and, properly interpreted, gives the best information on the burn-out of the jet. Thus since our fuel has been approximated in the form

$$\bar{\kappa}_1 = \sqrt{\frac{d}{x}}\, F'(n)\ k(x/d)$$

it will suffice to show the values of $k(x/d)$ and infer that the centerline fuel mass fraction,

$$\kappa_1(x,0) = \sqrt{\frac{d}{x}}\, F'(0)\, k(x/d) \qquad (128)$$

decreases somewhat more rapidly with x. Because the fuel concentration of the non-reacting jet will decrease as $\sqrt{d/x}$ along the axis [k(x/d) = 1], the observed decrease of k(x/d) with x is due only to the chemical reaction, rather than to the normal dilution due to mixing.

Figure 12 shows the value of k(x/d) in terms of distance from the fuel injection point for three different values of λ. It will be recalled that λ is the single additional universal constant that enters in the coherent flame model and is associated with the flame shortening mechanism. All three curves were computed for the equivalence ratio, $\phi = 1.0$. The geometry of the curves appear quite reasonable when compared with the experimental results shown in Figures 14 through 17 of Reference 3. The effect of λ is quite clear from our calculations. For large λ, the flame shortening process is accentuated which, in turn, leads to a low flame density and a long flame. Smaller values of λ produce a correspondingly denser flame structure and shorter flames. As Figure 12 indicates, the results are quite sensitive to λ and here it should be possible to obtain a reasonably good determination of the value of λ from the fuel jet experiments that are available. This systematic and detailed comparison has not yet been made, but a superficial examination would indicate the λ will be some where between 0.1 and 0.5.

Figure 13 is presented to show the effect of equivalence ratio, ϕ, on the flame length when the value of λ has been fixed. Clearly large equivalence ratios lead to long flames and low equivalence ratios lead to shorter ones. This behavior results from the relatively larger amount of oxidizer that must generally be entrained and mixed for a flame with high equivalence ratios than for one of low equivalence ratio. Familiar examples of high and low equivalence ratio are the methane-air flame and the hydrogen-air flame, respectively. The results of Figure 13, computed using the value $\lambda = 0.5$, suggest, upon comparison with the experiments, that a somewhat smaller value of λ would be appropriate.

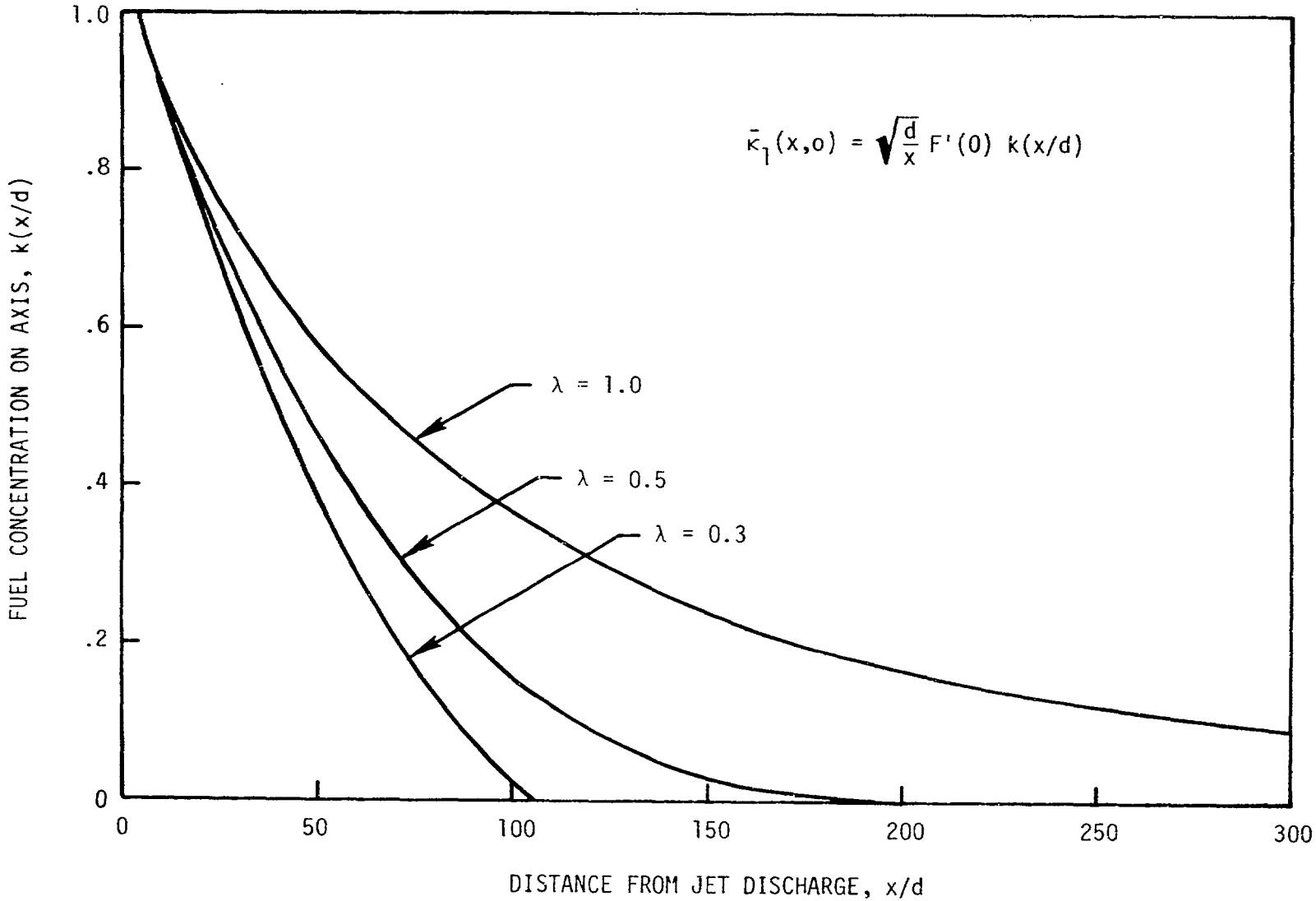

Figure 12. Effect of Flame Shortening Constant on Length of Turbulent Diffusion Flame from Fuel Jet. ϕ = 1.0.

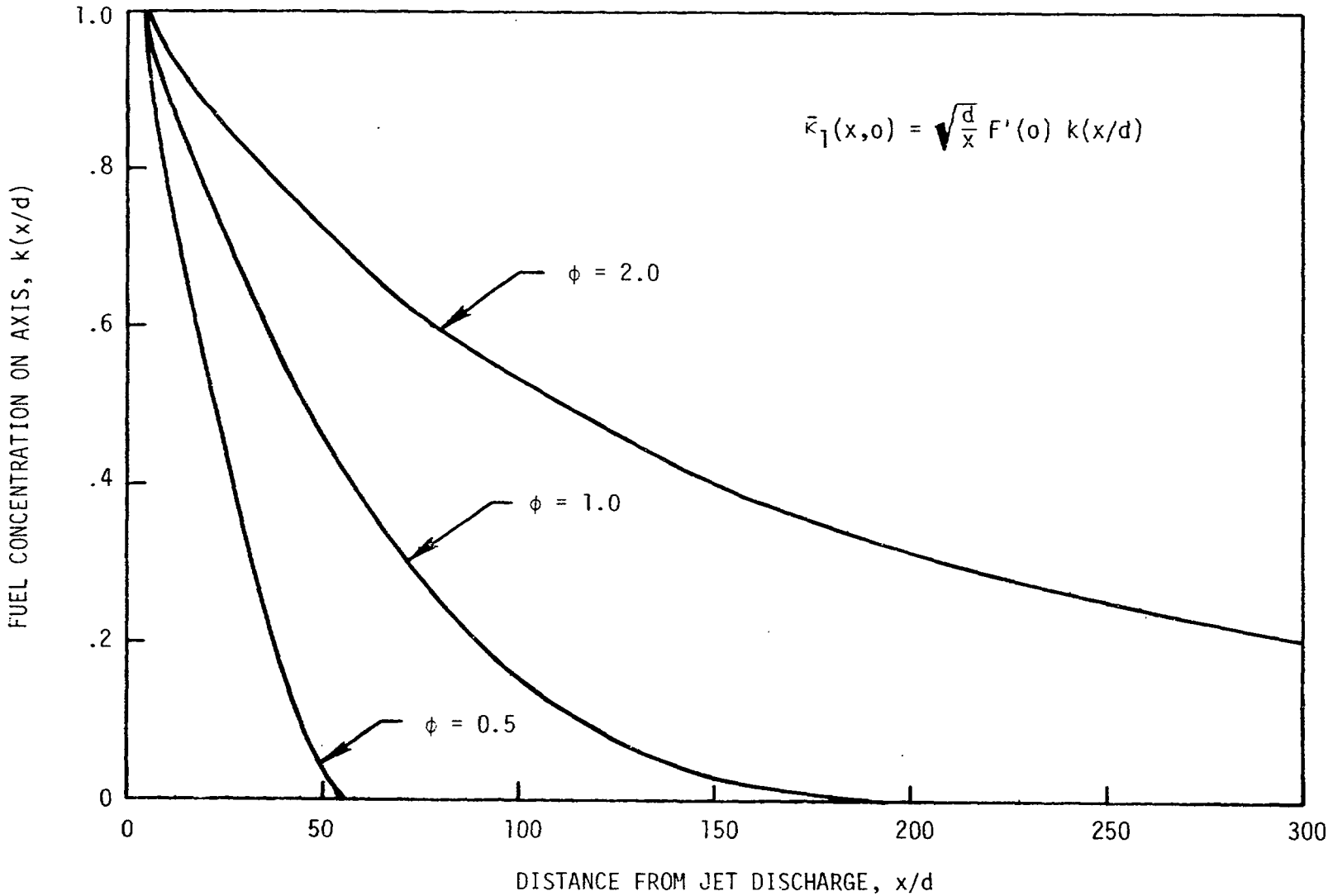

Figure 13. Effect of Equivalence Ratio on Length of Turbulent Diffusion Flame from Fuel Jet. λ = 0.5.

REFERENCES

1. Damköhler, G., 1940. Z. Electrochem. 46, p. 601.

2. Shchelkin, K. I., 1943. J. Tech. Phys. (USSR) 18, p. 520.

3. Hawthorne, W. R., Weddell, D. S., and Hottel, H. C., 1948. Proceedings, Third Symposium on Combustion, Flame, and Explosion Phenomena. Williams and Wilkens Co., Baltimore (1948), p. 266.

4. Hottel, H. C., 1952. Proceedings, Fourth Symposium (International) on Combustion. Williams and Wilkens Co., Baltimore (1952), p. 97.

5. Karlovitz, B., Denniston, D. W. Jr., and Wells, F. E., 1951. J. Chem. Phys. 19, p. 451.

6. Wohl, K., Shore, L., von Rosenberg, H., and Weil, C. W., 1952. Proceedings, Fourth Symposium (International) on Combustion. Williams and Wilkens Co., Baltimore (1952), p. 620.

7. Yamazaki, T. and Tsuji, H., 1960. Proceedings, Eighth Symposium (International) on Combustion. Williams and Wilkins Co., Baltimore (1960), p. 543.

8. Karlovitz, B., Denniston, D. W. Jr., Knapschaefer, D. H., and Wells, F. E., 1952. Proceedings, Fourth Symposium (International) on Combustion. Williams and Wilkins Co., Baltimore (1952), p. 613.

9. Becker, H. A., Hottel, H. C., and Williams, G. C., 1964. Proceedings, Tenth Symposium (International) on Combustion. The Combustion Institute (1964), p. 1253.

   Williams, G. C., Hottel, H. C., and Gurnitz, R. N., 1968. Proceedings, Twelfth Symposium (International) on Combustion. The Combustion Institute (1968), p. 1081.

10. Zukoski, E. E. and Marble, F. E., 1955. Combustion Researches and Reviews, 1955, AGARD, Paris. Butterworths Scientific Publications, p. 167.

    Zukoski, E. E. and Marble, F. E., 1956. Proceedings, Aerothermochemistry, Gas Dynamics Symposium. Northwestern University (1956), p. 205.

11. Brown, G. L. and Roshko, A., 1974. J. Fluid Mech. 64, pt. 4, p. 775.

12. Reynolds, O., 1894. Phil. Trans. Roy. Soc. A, Vol. 186 (1894). Papers, Vol. 2, p. 535.

13. Taylor, G. I., 1935. Proc. Roy. Soc. A, 151, p. 421.

14. Kármán, Th. von, 1938. Proc. Roy. Soc. A, 164, p. 192.

15. Witte, A. B., et al., 1975. TRW Final Report, AFWL-TR-75-266.

16. Carrier, G. F., Fendell, F. E., and Marble, F. E., 1975. SIAM J. Appl. Math. 28, No. 2, p. 453.

REFERENCES (Continued)

17. Batchelor, G. K., 1952. Proc. Roy. Soc. A 213, p. 349.

18. Saffman, P. G., 1970. Proc. Roy. Soc. A 317, p. 417.

    Saffman, P. G., 1974. Studies in Mathematics, Vol. LII, No. 1, Massachusetts Institute of Technology, p. 17.

    Milinazzo, F. and Saffman, P. G., 1976. Studies in Applied Math., No. 55 (1976), p. 45.

19. Kármán, Th. von, 1930. Nach. Gas. d. Wiss. Göttingen, Math-Phys. Klass, p. 59.

20. Witte, A. B. et al., 1974. TRW Final Report, AFWL-TR-74-78.

21. Blottner, F. G., 1970. AIAA Jour., 8, No. 2, p. 193.

22. Cummings, J. C., et al., 1977. Jour. of Quant. Spectroscopy and Radiative Transfer (to be published).

GOVERNMENT AGENCIES

1. British Embassy
   3100 Massachusetts Avenue, N.
   Washington, D.C. 20008
   ATTN: Mr. J. Barry Jam[illegible]
   Propulsion Offic

2. Central Intelligence Agency
   Washington, D.C. 20505
   ATTN: CRS/ADD/Publications

3. Institute for Defense Analyses
   400 Army-Navy Drive
   Arlington, Virginia 22202
   ATTN: Dr. Hans G. Wolfhard,
   Sen. Staff

4. Defense Documentation Center
   Cameron Station
   Alexandria, Virginia 22314

5. EPA Technical Center
   Research Triangle Park
   North Carolina 27711
   ATTN: Dr. W. Herget, P-222

6. Esso Research and Engineering Company
   Government Research Laboratory
   P.O. Box 8
   Linden, New Jersey 07036
   ATTN: Dr. William F. Taylor

7. Arnold Air Force Station
   Tennessee 36389
   ATTN: AEDC (DYF)

8. Arnold Air Force Station
   Tennessee 37389
   ATTN: R F. Smith, Jr., Chief
   T-Cells Division
   Engine Test Facility

9. Air Force Aero Propulsion Laboratory
   Wright-Patterson Air Force Base
   Ohio 45433
   ATTN: STINFO Office

10. Air Force Eastern Test Range
    MU-135
    Patrick Air Force Base
    Florida 32925
    ATTN: AFETR Technical Library

11. Air Force Office of Scientific Research
    Bolling Air Force Base, Building 410
    Washington, D.C. 20332
    ATTN: Dr. Joseph F. Masi

12. Air Force Aero Propulsion Laboratory
    Wright-Patterson AFB, Ohio 45433
    ATTN: AFAPL/TBC
    Dr. Kervyn Mach

13. Air Force Aero Propulsion Laboratory
    Wright-Patterson AFB, Ohio 45433
    ATTN: AFAPL/TBC
    Francis R. Ostdiek

14. Air Force Rocket Propulsion Laboratory
    Department of Defense
    Edwards AFB, California 93523
    ATTN: LKCG (Mr. Selph)

15. U.S. Army Air Mobility Research and
    Development Laboratory
    Eustis Directorate
    Fort Eustis, Virginia 23604
    ATTN: Propulsion Division
    (SAVDL-EU-PP)

16. U.S. Army Artillery Combat
    Developments Agency
    Fort Sill, Oklahoma 73503
    ATTN: Commanding Officer

17. U.S. Army Missile Command
    Redstone Arsenal, Alabama 35809
    ATTN: AMSMI-RR

18. U.S. Army Missile Command
    Redstone Scientific Information Center
    Redstone Arsenal, Alabama 35809
    ATTN: Chief, Document Section

19. Indiana State Library
    140 North Senate Avenue
    Indianapolis, Indiana 46204
    ATTN: Patricia Matkovic
    Reference Librarian
    Indiana Division

20. NASA Headquarters
    600 Independence
    Washington, D.C. 20546
    ATTN: Dr. Gordon Banerian

21. NASA Headquarters
    Aeronautical Propulsion Division
    Code RL, Deputy Director
    Office of Advanced Research & Technology
    Washington, D.C. 20546
    ATTN: Mr. Nelson F. Rekos

22. NASA Ames Research Center
    Deputy Chief Aeronautics Division
    Mail Stop 27-4
    Moffett Field, California 94035
    ATTN: Mr. Edward W. Perkins

23. NASA Ames Research Center
    Aerodynamics Branch 227-8
    Moffett Field, California 94305
    ATTN: Mr. Ira R. Schwartz

24. NASA Lewis Research Center
    21000 Brookpark Road
    Cleveland, Ohio 44135
    ATTN: D. Morris, Mail Stop 60-3

25. NASA Lewis Research Center
    Hypersonic Propulsion Section
    Mail Stop 6-1
    21000 Brookpark Road
    Cleveland, Ohio 44135
    ATTN: Dr. Louis A. Povinelli

26. NASA Marshall Space Flight Center
    S&E ASTN-P
    Huntsville, Alabama 35812
    ATTN: Mr. Keith Chandler

27. National Science Foundation
    Engineering Energetics
    Engineering Division
    Washington, D.C. 20550
    ATTN: Dr. George Lee

28. National Science Foundation
    Engineering Energetics
    Engineering Division
    Washington, D.C. 20550
    ATTN: Dr. M. Ojalvo

29. National Science Foundation
    Engineering Energetics
    Engineering Division
    Washington, D.C. 20550
    ATTN: Dr. Royal Rostenbach

30. Naval Air Development Center
    Commanding Officer (AD-5)
    Warminster, Pennsylvania 18974
    ATTN: NADC Library

31. Naval Air Propulsion Test Center (R&T)
    Trenton, New Jersey 08628
    ATTN: Mr. Al Martino

32. Naval Air Systems Command
Department of the Navy
Washington, D.C. 20360
ATTN: Research Administrator
AIR 310

33. Naval Air Systems Command
Department of the Navy
Washington, D.C. 20360
ATTN: Propulsion Technology Admin.
AIR 330

34. Naval Air Systems Command
Department of the Navy
Washington, D.C. 20360
ATTN: Technical Library Division
AIR 604

35. Naval Ammunition Depot
Research and Development Department
Building 190
Crane, Indiana 47522
ATTN: Mr. B.E. Douda

36. Naval Ordnance Laboratory Commander
White Oak
Silver Springs, Maryland 20910
ATTN: Library

37. Naval Ordnance Systems Command
Department of the Navy
Washington, D.C. 20360
ATTN: ORD 0331

38. Naval Postgraduate School
Department of Aeronautics, Code 57
Monterey, California 93940
ATTN: Dr. Allen E. Fuhs

39. Naval Postgraduate School
Library (Code 2124)
Monetrey, California 93940
ATTN: Superintendent

40. Naval Postgraduate School
Monterey, California 93940
ATTN: Library (Code 0212)

41. Office of Naval Research Branch Office
1030 East Green Street
Pasadena, California 91106
ATTN: Dr. Rudolph J. Marcus

42. Office of Naval Research Branch Office
536 South Clark Street
Chicago, Illinois 60605
ATTN: Commander

43. Office of Naval Research Branch Office
495 Summer Street
Boston, Massachusetts 02210
ATTN: Commander

44. Office of Naval Research
Power Branch, Code 473
Department of the Navy
Arlington, Virginia 22217

45. Office of Naval Research
Fluid Dynamics Branch, Code 438
Department of the Navy
Washington, D.C. 22217
ATTN: Mr. Morton Cooper

46. Naval Research Lab
Code 7710
Washington, D.C. 20390
ATTN: W.W. Bahwanz

47. Naval Research Laboratory Director
Washington, D.C. 20390
ATTN: Technical Information Division

48. Naval Research Laboratory Director
Washington, D.C. 20390
ATTN: Library Code 2629 (ONRL)

49. Naval Ship Research and Development Center
Annapolis Division
Annapolis, Maryland 21402
ATTN: Library, Code A214

50. Naval Ship Systems Command
Department of the Navy
Washington, D.C. 20360
ATTN: Technical Library

51. Naval Weapons Center Commander
China Lake, California 93555
ATTN: Airbreathing Propulsion Branch
Code 4583

52. Naval Weapons Center
Chemistry Division
China Lake, California 93555
ATTN: Dr. William S. McEwan
Code 605

53. Naval Weapons Center
Commander
China Lake, California 93555
ATTN: Technical Library

54. Naval Weapons Center
Code 608, Thermochemistry Group
China Lake, California 93555
ATTN: Mr. Edward W. Price, Head

55. Naval Weapons Laboratory
Dahlgren, Virginia 22448
ATTN: Technical Library

56. Naval Undersea Research and
Development Center
San Diego, California 92132
ATTN: Technical Library
Code 133D

57. Naval Underwater Systems Center
Fort Trumbull
New London, Connecticut 06320
ATTN: Technical Library

58. Naval Underwater Systems Center
Code 58-331
Newport, Rhode Island 02840
ATTN: Dr. Robert Lazar

59. Picatinny Arsenal
Commanding Officer
Dover, New Jersey 07801
ATTN: Technical Information Library

60. State Documents Section
Exchange and Gift Division
Washington, D.C. 20540
ATTN: Library of Congress

U.S. INDUSTRIES AND LABORATORIES

61. AeroChem Research Laboratories, Inc.
P.O. Box 12
Princeton, New Jersey 08540
ATTN: Dr. Arthur Fontijn

62. AeroChem Research Laboratories, Inc.
P.O. Box 12
Princeton, New Jersey 08540
ATTN: Library

63. Aerojet Liquid Rocket Company
P.O. Box 13222
Sacramento, California 95813
ATTN: Technical Information Center

64. Aeronautical Research Association
of Princeton
50 Washington Road
Princeton, New Jersey 08540
ATTN: Dr. C. Donaldson

65. Aeroprojects, Inc.
West Chester
Pennsylvania 19380

66. The Aerospace Corporation
P.O. Box 92957
Los Angeles, California 90009
ATTN: Mr. Alexander Muraszew

67. Atlantic Research Corporation
5390 Cherokee Avenue
Alexandria, Virginia 22314
ATTN: Dr. Andrej Macek

68. Atlantic Research Corporation
5390 Cherokee Avenue
Alexandria, Virginia 22314
ATTN: Librarian

69. Atlantic Research Corporation
5390 Cherokee Avenue
Alexandria, Virginia 22314
ATTN: Dr. Kermit E. Woodcock
Manager, Propulsion

70. Avco Everett Research Laboratory
Everett, Massachusetts 02149
ATTN: Librarian

71. Avco Lycoming Corporation
550 South Main Street
Stratford, Connecticut 06497
ATTN: Mr. John W. Schrader

72. Ballistics Research Laboratory
Commanding Officer
Aberdeen Proving Ground, Maryland 21005
ATTN: Library

73. Battelle
Columbus Laboratories
505 King Avenue
Columbus, Ohio 43201
ATTN: Mr. Abbott A. Putnam
Atmospheric Chemistry &
Combustion Systems Division

74. Beech Aircraft Corporation
9709 East Central
Wichita, Kansas 67201
ATTN: William M. Byrne, Jr.

75. Bell Aerospace Company
P.O. Box 1
Buffalo, New York 14240
ATTN: Technical Library

76. Bureau of Mines
Bartlesville Energy Research Center
Box 1398
Bartlesville, Oklahoma 74003

77. Calspan Corporation
4455 Genessee Street
Buffalo, New York 14221
ATTN: Head Librarian

78. Computer Genetics Corporation
Wakefield, Massachusetts 01880
ATTN: Mr. Donald Leonard
Technical Director

79. Convair Aerospace Division
Manager of Propulsion
P.O. Box 748
Fort Worth, Texas 76101
ATTN: L. H. Schreiber

80. Detroit Diesel Allison Division
P.O. Box 894
Indianapolis, Indiana 46206
ATTN: Dr. Sanford Fleeter

81. Dynalysis of Princeton
20 Nassau Street
Princeton, New Jersey 08540
ATTN: Dr. H.J. Herring

82. Fairchild Industries
Fairchild Republic Division
Farmingdale, New York 11735
ATTN: Engineering Library

83. Flame Research, Inc.
P.O. Box 10502
Pittsburgh, Pennsylvania 15235
ATTN: Dr. John Manton

84. Forest Fire and Engineering Research
Pacific Southwest Forest & Range
Experiment Station
P.O. Box 245
Berkeley, California 94701
ATTN: Assistant Director

85. Garrett Corporation
AiResearch Manufacturing Company
Sky Harbor Airport
402 South 36th Street
Phoenix, Arizona 85034
ATTN: Mr. Aldo L. Romanin, Mgr.
Aircraft Propulsion Engine
Product Line

86. General Dynamics
Electro Dynamic Division
P.O. Box 2507
Pomona, California 91766
ATTN: Library MZ 620

87. General Dynamics
P.O. Box 748
Fort Worth, Texas 76101
ATTN: Technical Library MZ 2246

88. General Electric Company
AEG Technical Information Center
Mail Drop N-32, Building 700
Cincinnati, Ohio 45215
ATTN: J.J. Brady

89. General Electric Company
SPO-Bldg, 174AE
1000 Western Avenue
West Lynn, Massachusetts 01910
ATTN: Mr. W. Bruce Gist

90. General Electric Space Sciences Lab
Valley Forge Space Technology Center
Room M-9144
P.O. Box 8555
Philadelphia, Pennsylvania 19101
ATTN: Dr. Theodore Baurer

91. General Motors Corporation
Detroit Diesel Allison Division
P.O. Box 894
Indianapolis, Indiana 46206
ATTN: Mr. P.C. Tram

92. General Motors Technical Center
Passenger Car Turbine Development
General Motors Engineering Staff
Warren, Michigan 48090
ATTN: T.F. Nagey, Director

93. Grumman Aerospace Corporation
Manager Space Vehicle Development
Bethpage, New York 11714
ATTN: Mr. O.S. Williams

94. Mr. Daniel L. Harshman
11131 Embassy Drive
Cincinnati, Ohio 45240

95. Hercules Incorporated
Allegany Ballistics Laboratory
P.O. Box 210
Cumberland, Maryland 21502
ATTN: Mrs. Louise S. Derrick
Librarian

96. Hercules Incorporated
P.O. Box 98
Magna, Utah 84044
ATTN: Library 100-H

97. LTV Vought Aeronautics Company
Flight Technology, Project Engineer
P.O. Box 5907
Dallas, Texas 75222
ATTN: Mr. James C. Utterback

98. Lockheed Aircraft Corporation
Lockheed Missiles and Space Company
Huntsville, Alabama 35804
ATTN: John M. Banefield
Supervisor Propulsion

99. Lockheed-Georgia Company
Dept. 72-47, Zone 259
Marietta, Georgia 30060
ATTN: William A. French

100. Lockheed Missiles and Space Company
3251 Hanover Street
Palo Alto, California 94304
ATTN: Palo Alto Library 52-52

101. Lockheed Propulsion Company
Scientific and Technical Library
P.O. Box 111
Redlands, California 92373
ATTN: Head Librarian

102. Los Alamos Scientific Laboratory
P.O. Box 1663
Los Alamos, New Mexico 87544
ATTN: J. Arthur Freed

103. The Marquardt Company
CCI Aerospace Corporation
16555 Saticoy Street
Van Nuys, California 91409
ATTN: Library

104. Martin-Marietta Corporation
P.O. Box 179
Denver, Colorado 90201
ATTN: Research Library 6617

105. Martin-Marietta Corporation
Orlando Division
P.O. Box 5837
Orlando, Florida 32805
ATTN: Engineering Library, mp-30

106. McDonnell Aircraft Company
P.O. Box 516
St. Louis, Missouri 63166
ATTN: Research & Engineering Library
Dept. 218 - Bldg. 101

107. McDonnell Douglas Corporation
Project Propulsion Engineer
Dept. 243, Bldg. 66, Level 25
P.O. Box 516
St. Louis, Missouri 63166
ATTN: Mr. William C. Paterson

108. McDonnell Douglas Astronautics Company
5301 Bolsa Avenue
Huntington Beach, California 92647
ATTN: A3-328 Technical Library

109. Nielsen Engineering and Research, Inc.
510 Clyde Avenue
Mountain View, California 94040
ATTN: Dr. Jack N. Nielsen

110. Northrop Corporation
Ventura Division
1515 Rancho Conejo Boulevard
Newbury Park, California 91230
ATTN: Technical Information Center

111. Mr. J. Richard Perrin
16261 Darcia Avenue
Encino, California 91316

112. Philco-Ford Corporation
Aeronutronic Division
Ford Road
Newport Beach, California 92663
ATTN: Technical Information Center

113. Pratt and Whitney Aircraft
Project Engineer, Advanced
Military System
Engineering Department - 2B
East Hartford, Connecticut 06108
ATTN: Mr. Donald S. Rudolph

114. Pratt and Whitney Aircraft Division
United Aircraft Company
400 South Main Street
East Hartford, Connecticut 06108
ATTN: Mr. Dana B. Waring
Manager-Product Technology

115. Pratt and Whitney Aircraft
Program Manager, Advanced
Military Engineer
Engineering Department - 2B
East Hartford, Connecticut 06108
ATTN: Dr. Robert I. Strough

116. Pratt and Whitney Aircraft
Florida Research and Development Company
P.O. Box 2691
West Palm Beach, Florida 33402
ATTN: Mr. William R. Alley
Chief of Applied Research

117. Rocket Research Corporation
11441 Willow Road
Redmond, Washington 98052
ATTN: Thomas A. Groudle

118. Rocketdyne Division
North American Rockwell
6633 Canoga Avenue
Canoga Park, California 91304
ATTN: Technical Information Center

119. Sandia Laboratories
P.O. Box 969
Livermore, California 94550
ATTN: Dr. Dan Hartley, Div. 8115

120. Sandia Laboratories
Livermore, California 94550
ATTN: Robert Gallagher

121. Sandia Laboratories
P.O. Box 5800
Albuquerque, New Mexico 87115
ATTN: Technical Library, 3141

122. Solar
2200 Pacific Highway
San Diego, California 92112
ATTN: Librarian

123. Standard Oil Company (Indiana)
P.O. Box 400
Naperville, Illinois 60540
ATTN: R. E. Pritz

124. Stauffer Chemical Company
Richmond, California 94802
ATTN: Dr. J. H. Morgenthaler

125. Teledyne CAE
1330 Laskey Road
Toledo, Ohio 43601
ATTN: Technical Library

126. TRW Systems
One Space Park
Redondo Beach, California 90278
ATTN: Mr. F.E. Fendell (R1/1004)

127. TRW Systems Group
One Space Park
Bldg. 0-1 Room 2080
Redondo Beach, California 90278
ATTN: Mr. Donald H. Lee Manager

128. United Technologies Research Center
East Hartford, Connecticut 06108
ATTN: Librarian

129. Valley Forge Sapce Technology Center
P.O. Box 8555
Philadelphia, Pennsylvania 19101
ATTN: Dr. Bert Zauderer

130. Vought Missiles and Space Company
P.O. Box 6267
Dallas, Texas 75222
ATTN: Library - 3-41000

131. Boston College
Department of Chemistry
Chestnut Hill, Massachusetts 02167
ATTN: Rev. Donald MacLean, S.J.
Associate Professor

132. Brown University
Division of Engineering
Box D
Providence, Rhode Island 02912
ATTN: Dr. R. A. Dobbins

133. California Institute of Technology
Department of Chemical Engineering
Pasadena, California 91109
ATTN: Professor W. H. Corcoran

134. California Institute of Technology
Jet Propulsion Laboratory
4800 Oak Grove Drive
Pasadena, California 91103
ATTN: Library

135. University of California, San Diego
Dept. of Engineering Physics
P.O. Box 109
La Jolla, California 92037
ATTN: Professor S.S. Penner

136. University of California
School of Engineering and
Applied Science
7513 Boelter Hall
Los Angeles, California 90024
ATTN: Engineering Reports Group

137. University of California
Lawrence Radiation Laboratory
P.O. Box 808
Livermore, California 94550
ATTN: Technical Information Dept. L-3

138. University of California
General Library
Berkeley, California 94720
ATTN: Documents Department

139. Case Western Reserve University
10900 Euclid Avenue
Cleveland, Ohio 44106
ATTN: Sears Library - Reports
Department

140. Case Western Reserve University
Division of Fluid Thermal and
Aerospace Sciences
Cleveland, Ohio 44106
ATTN: Professor Eli Reshotko

141. Colorado State University
Engineering Research Center
Fort Collins, Colorado 80521
ATTN: Mr. V. A. Sandborn

142. The University of Connecticut
Department of Mechanical Engineering
U-139
Storrs, Connecticut 06268
ATTN: Professor E. K. Dabora

143. Cooper Union
School of Engineering and Science
Cooper Square
New York, New York 10003
ATTN: Dr. Wallace Chintz
Associate Professor of ME

144. Cornell University
Department of Chemistry
Ithaca, New York 14850
ATTN: Professor Simon H. Bauer

145. Franklin Institute Research Laboratories
Philadelphia, Pennsylvania 19103
ATTN: Dr. G.P. Wachtell

146. George Washington University
Washington, D.C. 20052
ATTN: Dr. Robert Goulard
Dept. of Civil, Mechanical and
Environmental Engineering

147. George Washington University Library
Washington, D.C. 20006
ATTN: Reports Section

148. Georgia Institute of Technology
Atlanta, Georgia 30332
ATTN: Price Gilbert Memorial Library

149. Georgia Institute of Technology
School of Aerospace Engineering
Atlanta, Georgia 30332
ATTN: Dr. Ben T. Zinn

150. University of Illinois
Department of Energy Engineering
Box 4348
Chicago, Illinois 60680
ATTN: Professor Paul H. Chung

151. University of Illinois
College of Engineering
Department of Energy Engineering
Chicago, Illinois 60680
ATTN: Dr. D. S. Hacker

152. The Johns Hopkins University
Applied Physics Laboratory
Johns Hopkins Road
Laurel, Maryland 20810
ATTN: Chemical Propulsion
Information Agency

153. The Johns Hopkins University
Applied Physics Laboratory
Johns Hopkins Road
Laurel, Maryland 20810
ATTN: Document Librarian

154. The Johns Hopkins University
Applied Physics Laboratory
Johns Hopkins Road
Laurel, Maryland 20810
ATTN: Dr. A. A. Westenberg

155: University of Kentucky
Department of Mechanical Engineering
Lexington, Kentucky 40506
ATTN: Dr. Robert E. Peck

156. Massachusetts Institute of Technology
Department of Chemical Engineering
Cambridge, Massachusetts 02139
ATTN: Dr. Jack B. Howard

157. Massachusetts Institute of Technology
Libraries, Room 14 E-210
Cambridge, Massachusetts 02139
ATTN: Technical Reports

158. Massachusetts Institute of Technology
Room 10-408
Cambridge, Massachusetts 02139
ATTN: Engineering Technical Reports

159. Massachusetts Institute of Technology
Dept. of Mechanical Engineering
Room 3-350
Cambridge, Massachusetts 02139
ATTN: Dr. M. Cardillo

160. Massachusetts Institute of Technology
Dept. of Mechanical Engineering
Room 3-246
Cambridge, Massachusetts 02139
ATTN: Professor James Fay

161. Midwest Research Institute
425 Volker Boulevard
Kansas City, Missouri 64100
ATTN: Dr. T. A. Milne

162. New Mexico State University
Dept. of Mechanical Engineering
Box 3450
Las Cruces, New Mexico 88003
ATTN: Dr. Dennis M. Zallen

163. New York Institute of Technology
Wheatley Road
Old Westbury, New York 11568
ATTN: Dr. Fox

164. University of North Carolina
Periodicals and Serials Division
Drawer 870 Library
Chapel Hill, North Carolina 27514
ATTN: Mr. Stephen Berk

165. University of Notre Dame
Serials Record
Memorial Library
Notre Dame, Indiana 46556
ATTN: B. McIntosh

166. University of Notre Dame
College of Engineering
Notre Dame, Indiana 46556
ATTN: Dr. Stuart T. McComas
Assistant Dean for Research
and Special Projects

167. Ohio State University
Dept. of Chemical Engineering
140 West 19th Avenue
Columbus, Ohio 43210
ATTN: Dr. Robert S. Brodkey

168. The Pennsylvania State University
Room 207, Old Main Building
University Park, Pennsylvania 16802
ATTN: Office of Vice President
for Research

169. Princeton University
Dept. of Aerospace and Mechanical
Sciences
James Forrestal Campus
Princeton, New Jersey 08540
ATTN: Dr. Martin Summerfield

170. Princeton University
James Forrestal Campus Library
P.O. Box 710
Princeton, New Jersey 08540
ATTN: V. N. Simosko, Librarian

171. Rice University
Welch Professor of Chemistry
Houston, Texas 77001
ATTN: Dr. Joseph L. Franklin

172. University of Rochester
Dept. of Chemical Engineering
Rochester, New York 14627
ATTN: Dr. John R. Ferron

173. Stanford University
Dept. of Aeronautics and Astronautics
Stanford, California 94305
ATTN: Dr. Walter G. Vincenti

174. State University of New York - Buffalo
Dept. of Mechanical Engineering
228 Parker Engineering Building
Buffalo, New York 14214
ATTN: Dr. George Rudinger

175. Stevens Institute of Technology
Department of Mechanical Engineering
Castle Point Station
Hoboken, New Jersey 07030
ATTN: Professor Fred Sisto

176. University of Virginia
Department of Aerospace Engineering
School of Engineering and Applied Science
Charlottesville, Virginia 22901
ATTN: Dr. John E. Scott

177. University of Virginia
Science/Technology Information Center
Charlottesville, Virginia 22901
ATTN: Dr. Richard H. Austin

178. Yale University
Mason Laboratory
9 Hillhouse Avenue
New Haven, Connecticut 06520
ATTN: Professor Peter P. Wegener

FOREIGN INSTITUTIONS

179. A/S Kongsberg Vaapenfabrikk
Gas Turbine Division
3601 Konsber, NORWAY
ATTN: R.E. Stanley
Senior Aerodynamicist

180. Conservatoire National des Arts
et Metiers
292, Rue Saint'Martin
75141 Paris Cedex 03, FRANCE
ATTN: Professor J. Gossee
Chaire de Thermique

181. DFVLR-Forschungszentrum Gottingen
Institut Fur Stromungsmechanik
Abteilung Theoretische Gashynamik
D-3400 Gottingen
Bunsenstrabe 10, GERMANY
ATTN: Professor Klaus Oswatitsch

182. Ecole Royale Militaire
30 Avenue de la Resaissance
Bruxelles B-1040, BELGIUM
ATTN: Professor Emile Tits

183. Fysisch Laboratorium
Fijksuniversiteit Utrecht
Sorbonnelaan, Utrecht,
THE NETHERLANDS
ATTN: Dr. F. Van der Valk

184. Imperial College
Department of Chemical Engineering
London SW7, ENGLAND
ATTN: Professor F. J. Weinberg

185. Imperial College of Science
and Technology
Department of Mechanical Engineering
Exhibition Road
London, SW7, ENGLAND
ATTN: Professor Gaydon

186. Imperial College of Science
and Technology
Department of Mechanical Engineering
Exhibition Road
London SW7, ENGLAND
ATTN: D. B. Spalding

187/1 Laboratoire de Mecanique des Fluides
36, Route de Dardilly, 36
B.P. No. 17
69130 Ecully, FRANCE
ATTN: G. Assassa

187/2 Laboratoire de Mecanique des Fluides
Ecole Centrale Lyonnaise
36, Route de Dardilly
69130 Ecully, FRANCE
ATTN: Dr. K. Papiliou

188. Ministry of Defense
Main Building, Room 2165
Whitehall Gardens
London SW1, ENGLAND
ATTN: Mr. L.D. Nicholson ED, idc
Vice Controller of Aircraft
Procurement Executive

189. Mitglied des Vorstands der Fried
Krumpp CmbH
43 Essen, Altendorferstrabe 103
GERMANY
ATTN: Professor Dr.-Ing.
Wilhelm Dettmering

190. National Aerospace (NLR)
Voorsterweg 31
Noord-Oost-Polder-Emmelord
THE NETHERLANDS
ATTN: Mr. F. Jaarsma

191. National Research Council
Division of Mechanical Engineering
Montreal Road, Ottawa
Ontario, CANADA KIA OR6
ATTN: Dr. R.B. Whyte

192. Nissan Motor Co., LTD.
3-5-1, Momoi, Suginami-Ku
Tokyo, JAPAN 167
ATTN: Dr. Y. Toda

193. Norweigian Defense Research Establishment
Superintendent NDRE
P.O. Box 25
2007 Kjeller, NORWAY
ATTN: Mr. T. Krog

194. ONERA
Energie and Propulsion
29 Avenue de la Division Leclure
92 Chatillon sous Bagneux, FRANCE
ATTN: Mr. M. Barrere

195. ONERA
Energie and Propulsion
29 Avenue de la Division Leclure
92 Chatillon sous Bagneux, FRANCE
ATTN: Mr. J. Fabri

196. ONERA
Energie and Propulsion
29 Avenue de la Division Leclure
92 Chatillon sous Bagneux, FRANCE
ATTN: Mr. Viaud

197. ONERA-DED
External Relations and Documentation
Department
29, Avenue de la Division Leclure
92320 Chatillon, sous Bagneux, FRANCE
ATTN: Mr. M. Salmon

198. Orta Dogu Teknik Universities
Mechanical Engineering Department
Ankara, TURKEY
ATTN: Professor H. Sezgen

199. Queen Mary College
Department of Mechanical Engineering
Thile Eld Road
London El, ENGLAND
ATTN: Professor M. W. Thring

200. Rolls-Royce (1971) Limited
Derby Engine Division
P.O. Box 31
Derby DE2 8BJ
London, ENGLAND
ATTN: C. Freeman, Installation
Research Department

201. Rome University
Via Bradano 28
00199 Rome, ITALY
ATTN: Professor Gaetano Salvatore

202. Sener
Departamentao de Investigation
Km. 22.500 de la antigua carretera
Madrid - Barcelona, SPAIN
ATTN: Mr. J. T. Diez Roche

203. Service Technique Aeronautique Moteurs
4 Avenue de la Parte d'Issy
75753 Paris Cedex 15, FRANCE
ATTN: Mr. M. Pianko, Ing. en chef

204. The University of Sheffield
Dept. of Chemical Engineering
and Fuel Technology
Mappin Street, Sheffield S1 3JD
ENGLAND
ATTN: Dr. Norman Chigier

205. Sophia University
Science and Engineering Faculty
Kioi 7 Tokyo-Chiyoda JAPAN 102
ATTN: Professor M. Susuki

206. The University of Sydney
Dept. of Mechanical Engineering
N.S.W. 2006
Sydney, AUSTRALIA
ATTN: Professor R. W. Bilger

207. Technical University of Denmark
Fluid Mechanics Department
Building 404 2800 Lyngby
DK-DENMARK
ATTN: Professor K. Refslund

208. University of Leeds
Leeds, ENGLAND
ATTN: Professor Dixon-Lewis

209. Universite de Poitiers Laboratoire
D'energetique et de Detonique
(L.A. au C.N.R.S. No. 193)
ENSMA - 86034 Poitiers, FRANCE
ATTN: Professor N. Manson

210. University of Tokyo
Department of Reaction Chemistry
Faculty of Engineering
Bunkyo-ku
Tokyo, JAPAN 113
ATTN: Professor T. Hikita

211. Vrije Universiteit Brussel
Fac. Toeg. Wetenshch.
A. Buyllaan 105
1050 Brussels, BELGIUM
ATTN: Ch. Hirsch

PROJECT SQUID CONTRACTORS
1975-76 and 1976-77 (New)

212. AeroChem Research Laboratory, Inc.
Reaction Kinetics Group
P.O. Box 12
Princeton, New Jersey 08540
ATTN: Dr. Arthur Fontijn

213. Aeronautical Research Associates of
Princeton, Inc.
P.O. Box 2229
50 Washington Road
Princeton, New Jersey 08540
ATTN: Dr. Ashok K. Varma

214. California Institute of Technology
Div. of Engineering and
Applied Science
Mail Stop 205-50
Pasadena, California 91109
ATTN: Dr. Anatol Roshko

215. Case Western Reserve University
Div. of Fluid, Thermal and Aerospace
Sciences
Cleveland, Ohio 44106
ATTN: Dr. J.S. T'ien

216. Colorado State University
Engineering Research Center
Foothills Campus
Fort Collins, Colorado 80521
ATTN: Dr. Willy Z. Sadeh

217. General Electric Company
Corporate Research and Development
P.O. Box 8
Schenectady, New York 12301
ATTN: Dr. Marshall Lapp

218. Massachusetts Institute of Technology
Chemistry Department, Room 6-123
77 Massachusetts Avenue
Cambridge, Massachusetts 02139
ATTN: Dr. John Ross

219. Michigan State University
Department of Mechanical Engineering
East Lansing, Michigan 48824
ATTN: Dr. John Foss

220. Pennsylvania State University
Applied Research Laboratory
University Park, Pennsylvania 16802
ATTN: Dr. Edgar P. Bruce

221. Polytechnic Institute of New York
Department of Aerospace Engineering
and Applied Mechanics
Farmingdale, New York 11735
ATTN: Dr. Samuel Lederman

222. Southern Methodist University
Thermal and Fluid Sciences Center
Institute of Technology
Dallas, Texas 75275
ATTN: Dr. Roger L. Simpson

223. Stanford University
Mechanical Engineering Department
Stanford, California 94305
ATTN: Dr. James P. Johnston

224. Stanford University
Mechanical Engineering Department
Stanford, California 94305
ATTN: Dr. S. J. Kline

225. Stanford University
Mechanical Engineering Department
Stanford, California 94305
ATTN: Dr. Sidney Self

226. TRW Systems
Engineering Sciences Laboratory
One Space Park
Redondo Beach, California 90278
ATTN: Dr. J. E. Broadwell

227. United Technologies Research Center
400 Main Street
East Hartford, Connecticut 06108
ATTN: Mr. Franklin O. Carta

228. United Technologies REsearch Center
400 Main Street
East Hartford, Connecticut 06108
ATTN: Dr. Alan C. Eckbreth

229. University of California - San Diego
Department of Aerospace and
Mechanical Engineering
La Jolla, California 92037
ATTN: Dr. Paul Libby

230. University of Colorado
Department of Aerospace
Engineering Sciences
Boulder, Colorado 80304
ATTN: Dr. Mahinder S. Uberoi

231. University of Michigan
Department of Aerospace Engineering
Ann Arbor, Michigan 48105
ATTN: Dr. T. C. Adamson, Jr.

232. University of Michigan
Department of Aerospace Engineering
Ann Arbor, Michigan 48105
ATTN: Dr. Martin Sichel

233. University of Missouri - Columbia
Department of Chemistry
Columbia, Missouri 65201
ATTN: Dr. Anthony Dean

234. University of Southern California
Department of Aerospace Engineering
University Park
Los Angeles, California 90007
ATTN: Dr. F. K. Browand

235. University of Washington
Department of Mechanical Engineering
Seattle, Washington 98195
ATTN: Dr. F.B. Gessner

236. Virginia Polytechnic Institute and
State University
Mechanical Engineering Department
Blacksburg, Virginia 24601
ATTN: Dr. Walter F. O'Brien, Jr.

237. Virginia Polytechnic Institute and
State University
Mechanical Engineering Department
Blacksburg, Virginia 24061
ATTN: Dr. Hal L. Moses

238. Yale University
Engineering and Applied Science
Mason Laboratory
New Haven, Connecticut 06520
ATTN: Dr. John B. Fenn

PURDUE UNIVERSITY

239. School of Aeronautics and Astronautics
Grissom Hall
West Lafayette, Indiana 47907
ATTN: Library

240. School of Mechanical Engineering
Mechanical Engineering Building
West Lafayette, Indiana 47907
ATTN: Library

241-250. Purdue University Advisors

UNCLASSIFIED

SECURITY CLASSIFICATION OF THIS PAGE (When Data Entered)

(9) Final rept 1 mar 75-31 Jan 77,

REPORT DOCUMENTATION PAGE

READ INSTRUCTIONS BEFORE COMPLETING FORM

1. REPORT NUMBER: (14) SQUID-TRW-9-PU
2. GOVT ACCESSION NO.
3. RECIPIENT'S CATALOG NUMBER

4. TITLE (and Subtitle): (6) THE COHERENT FLAME MODEL FOR TURBULENT CHEMICAL REACTIONS
5. TYPE OF REPORT & PERIOD COVERED: Final Technical 3-1-75 thru 1-31-77
6. PERFORMING ORG. REPORT NUMBER: 29314-6001-RU-00

7. AUTHOR(s): (10) Frank E. Marble, James E. Broadwell
8. CONTRACT OR GRANT NUMBER(s): 4965-52 and 8960-18

9. PERFORMING ORGANIZATION NAME AND ADDRESS: TRW Defense and Space Systems Group, One Space Park, Redondo Beach, California 90278
10. PROGRAM ELEMENT, PROJECT, TASK AREA & WORK UNIT NUMBERS: (15) N00014-75-C-1143

11. CONTROLLING OFFICE NAME AND ADDRESS: Project SQUID, Chaffee Hall, Purdue University, West Lafayette, Indiana 47907
12. REPORT DATE: (11) January 1977
13. NUMBER OF PAGES: (12) 51p. 54

14. MONITORING AGENCY NAME & ADDRESS (if different from Controlling Office): Office of Naval Research, Power Program, Code 473, 800 No. Quincy Street, Arlington, Virginia 22217
15. SECURITY CLASS. (of this report): Unclassified
15a. DECLASSIFICATION/DOWNGRADING SCHEDULE

16. DISTRIBUTION STATEMENT (of this Report)

Unclassified; distribution unlimited.

17. DISTRIBUTION STATEMENT (of the abstract entered in Block 20, if different from Report)

18. SUPPLEMENTARY NOTES

19. KEY WORDS (Continue on reverse side if necessary and identify by block number)

turbulent combustion
diffusion flames
turbulent chemical reactions
turbulent fuel jet
turbulent shear flow

20. ABSTRACT (Continue on reverse side if necessary and identify by block number)

A description of the turbulent diffusion flame is proposed in which the flame structure is composed of a distribution of laminar diffusion flame elements, whose thickness is small in comparison with the large eddies. These elements retain their identity during the flame development; they are strained in their own plane by the gas motion, a process that not only extends their surface area, but also establishes the rate at which a flame element consumes the reactants. Where this flame stretching process

DD FORM 1 JAN 73 1473 EDITION OF 1 NOV 65 IS OBSOLETE

UNCLASSIFIED 403617

has produced a high flame surface density, the flame area per unit volume, adjacent flame elements may consume the intervening reactant, thereby annihilating both flame segments. This is the flame shortening mechanism which, in balance with the flame stretching process, establishes the local level of the flame density. The consumption rate of reactant is then given simply by the product of the local flame density and the reactant consumption rate per unit area of flame surface. The proposed description permits a rather complete separation of the turbulent flow structure, on one hand, and the flame structure, on the other, and in this manner permits the treatment of reactions with complex chemistry with a minimum of added labor. The structure of the strained laminar diffusion flame may be determined by analysis, numerical computation, and by experiment without significant change to the model.

The flame density and the mass fractions of reactant are described by non-linear diffusion equations in which those equations for the reactants each contain a consumption or production term proportional to the local flame density. The flame density equation contains a production term associated with flame surface stretching and a consumption term describing the flame shortening by mutual annihilation. Each of the equations contains a turbulent diffusion term utilizing a scalar diffusivity. The model of inhomogeneous turbulence, proposed by Saffman, completes the description of the problem and couples with the flame and composition equations to determine the velocity distribution and the turbulent diffusivity. A single additional universal constant, over those appearing in Saffman's model, is required in the model equations for the flame.

The coherent flame model has been applied to diffusion flame structure in the mixing region between two streams and predicts correctly the result that the reactant consumption per unit length of flame is independent of the distance from the initiation of mixing. In this example which is carried out for small density changes, both the fluid mechanical and flame variables possess similarity solutions.

The coherent flame model is also applied to the turbulent fuel jet which clearly does not have a similarity solution simply because the finite mass flow of fuel is eventually consumed. The problem is solved utilizing an integral technique and numerical integration of the resulting differential equations. The model predicts the flame length and superficial comparison with experiments suggest a value for the single universal constant. The theory correctly predicts the change of flame length with changes in stoichiometric ratio for the chemical reaction.